HHS Public Access

Author manuscript

Nat Immunol. Author manuscript; available in PMC 2018 March 11.

Published in final edited form as:

Nat Immunol. 2017 November ; 18(11): 1249–1260. doi:10.1038/ni.3837.

Dynamic regulation of T Follicular Regulatory cell responses by interleukin 2 during influenza infection

Davide Botta[1], **Michael J. Fuller**[2], **Tatiana T. Marquez-Lago**[3,4], **Holly Bachus**[2], **John. E. Bradley**[2], **Amy S. Weinmann**[1], **Allan. J. Zajac**[1], **Troy D. Randall**[2], **Frances E. Lund**[1], **Beatriz León**[1], and **André Ballesteros-Tato**[2]

[1]Department of Microbiology, University of Alabama at Birmingham, Birmingham, Alabama, USA

[2]Department of Medicine, Division of Clinical Immunology and Rheumatology, University of Alabama at Birmingham, Alabama, USA

[3]Informatics Institute, University of Alabama at Birmingham, Alabama, USA

[4]Department of Genetics, University of Alabama at Birmingham, Alabama, USA

SUMMARY

Interleukin 2 (IL-2) promotes Foxp3$^+$-regulatory T (T_{reg}) cell responses, but inhibits T follicular helper (T_{FH}) cell development. However, it is not clear how IL-2 affects T follicular regulatory (T_{FR}) cells, a cell type with properties of both T_{reg} and T_{FH} cells. Using an influenza infection model, we demonstrated that high IL-2 concentrations at the peak of the infection prevented T_{FR} cell development by a Blimp-1–dependent mechanism. However, once the immune response resolved, some T_{reg} cells down-regulated CD25, up-regulated Bcl-6 and differentiated into T_{FR} cells, which then migrated into the B cell follicles to prevent the expansion of self-reactive B cell clones. Thus, unlike its effects on conventional T_{reg} cells, IL-2 inhibits T_{FR} cell responses.

INTRODUCTION

Interleukin-2 (IL-2) is essential for the development and maintenance of Foxp3$^+$CD4$^+$ T regulatory (T_{reg}) cells, which prevent autoimmune disease development[1]. The principal mechanism by which IL-2 promotes T_{reg} cell development is by triggering STAT5 activation, which binds to the *Foxp3* locus and promotes Foxp3 expression[2–4]. IL-2 signaling is also required to maintain the competitive fitness of T_{reg} cells in secondary lymphoid organs[5,6] and for reinforcing their suppressive activity[7,8]. Hence, mice lacking IL-2 or IL-2Rα (CD25) fail to maintain peripheral tolerance and develop autoimmune disease[9].

Correspondence should be addressed to A.B.-T. (aballest@uab.edu).

AUTHOR CONTRIBUTIONS.

A.B.-T. designed and performed the experiments with help from B.L., H.B., M.J.F., J.E.B. and D.B. A.B.-T., D.B. and B.L. analyzed the data. T.T.M-L. and A.S.W. analyzed the RNAseq data. A.B.-T. wrote the manuscript. D.B. and B.L. contributed to data interpretation and manuscript editing. A.J.Z. performed LCMV infections. T.D.R. and F.E.L. contributed to manuscript editing and discussion, and provided reagents that were critical to this work. All authors reviewed the manuscript before submission.

T_{reg} cells express high amounts of CD25, the α chain of the high-affinity IL-2 receptor, allowing them to effectively compete with other cells for available IL-2[10–12]. Indeed, IL-2-consumption by T_{reg} cells is one of the main mechanisms by which they prevent effector-T cell (T_{eff}) responses[13]. Conversely, IL-2 consumption by T_{reg} cells facilitates $CD4^+$ T follicular helper (T_{FH}) cell development[10], since IL-2 signaling inhibits T_{FH} cell differentiation[14–16]. Interestingly, some activated T_{reg} cells down-regulate CD25, and do not require IL-2 for their homeostatic maintenance[17]. Instead, their survival is dependent on ICOS–ICOS-L interactions[17]. Similarly, antigen-experienced T_{reg} cells in the skin[18] and in aged mice[19] express less CD25, and depend on IL-7 and IL-15 rather than IL-2 for their maintenance, thus suggesting that IL-2 might be dispensable for the homeostasis of some T_{reg} cell subsets.

Interestingly, some Foxp3-expressing T_{reg} cells up-regulate Bcl-6 and CXCR5, molecules that are normally expressed by T_{FH} cells[20,21]. These $Foxp3^+Bcl\text{-}6^+CXCR5^+CD4^+$ cells are known as T follicular regulatory (T_{FR}) cells[20–22], which home to B cell follicles where they suppress B cell responses[20–25]. The ability of T_{FR} cells to co-express Foxp3 and Bcl-6 is somewhat surprising, as IL-2 signaling is important for Foxp3 expression, but inhibits Bcl-6[14,15,26]. Thus, it is unclear how IL-2 might be involved in the differentiation or maintenance of T_{FR} cells.

In this study, we investigated the role of IL-2 in T_{FR} cell responses to influenza. We demonstrated that high concentrations of IL-2 at the peak of the infection promoted the expression of Blimp-1 in T_{reg} cells, which suppressed Bcl-6 expression and thereby precluded T_{FR} cell development. As a consequence, T_{FR} cells failed to accumulate at the peak of the influenza infection. However, once the virus was eliminated and the IL-2 concentrations declined, some $CD25^{hi}$ T_{reg} cells down-regulated CD25, up-regulated Bcl-6 and differentiated into T_{FR} cells, which migrated into the B cell follicles to prevent the accumulation of self-reactive B cell clones. Collectively, our data demonstrate that IL-2 signaling differentially controls conventional T_{reg} and T_{FR} cell responses to influenza virus, and reveal an important role for T_{FR} cells in maintaining B-cell tolerance after influenza infection.

RESULTS

Kinetics of T_{FR} cell expansion upon influenza infection

To evaluate whether T_{FR} cells could be detected after influenza infection, C57BL/6 (B6) mice were intranasally (i.n) infected with influenza A/PR8/34 (PR8) and $Foxp3^+CD4^+$ T cells were characterized in the lung-draining mediastinal lymph node (mLN) 30 days later (Fig. 1a–c). $Foxp3^+CD69^{lo}CD4^+$ cells expressed low amounts of Bcl-6 and CXCR5 (Fig. 1a). In contrast, $Foxp3^+CD69^{hi}CD4+$ T cells could be separated into $Bcl\text{-}6^{lo}CXCR5^{lo}$ cells, which were $PD\text{-}1^{lo}$ and $GL\text{-}7^{lo}$, and $Bcl\text{-}6^{hi}CXCR5^{hi}$ cells, which were $PD\text{-}1^{hi}$ and $GL\text{-}7^{hi}$ (Fig. 1a–c). Thus, we designated the $Bcl\text{-}6^{lo}CXCR5^{lo}Foxp3^+CD4^+$ T cells as conventional T_{reg} cells and $Bcl\text{-}6^{hi}CXCR5^{hi}Foxp3^+CD4^+$ T cells as T_{FR} cells. T_{FR} cell development requires SAP-mediated interaction with B cells[21]. As such, the frequency and number of $Bcl\text{-}6^{hi}CXCR5^{hi}$ T_{FR} cells were decreased in SAP-deficient (B6.$Sh2d1a^{-/-}$) mice relative to B6 mice (Fig. 1d,e). Finally, to show that $Foxp3^+$ cells homed to GCs following influenza

infection, we determined the placement of Foxp3$^+$ cells relative to B cell follicles and GCs in sections of mLNs obtained from day 30 influenza-infected mice (Supplementary Fig. 1a). As expected, we identified CD4$^+$Foxp3$^+$ cells within the B cell follicles, the interfollicular area and inside the GCs (Supplementary Fig. 1a,b). These results indicated that *bona fide* T_{FR} cells did develop following influenza virus infection.

We next infected B6 mice with influenza and enumerated T_{FR} cells and conventional T_{reg} cells in the mLN at different times after infection (Fig. 1f–h). Bcl-6^{hi}CXCR5^{hi} T_{FR} cells were barely detectable at the peak of the infection (day 7 to 15), but largely accumulated during the late phase of the primary response (day 30 to 60) (Fig. 1f,g). In contrast, conventional T_{reg} cells rapidly expanded between days 3 and 7 (Fig. 1h). Importantly, the paucity of T_{FR} cells at the peak of the infection was not due to a lack of GC B cells, since GC B cells were easily detected at day 10, continued to expand through day 15, and declined thereafter (Fig. 1i,j). We also observed that Bcl-6^{hi}CXCR5^{hi} T_{FH} cells (Fig. 1k,l) peaked between days 7 and 15 after infection, and subsequently contracted between days 15 and 30. Thus, in contrast to GC cells, T_{FH} cells and conventional T_{reg} cells, T_{FR} cells failed to accumulate at the peak of the infection.

To further confirm this conclusion, we evaluated the presence of Foxp3$^+$ cells within the GCs at days 10 and 30 after infection by immunohistochemistry (Supplementary Fig. 1c). Foxp3$^+$ cells were easily detected in the B cell follicles, interfollicular area and GCs on day 30. By contrast, very few Foxp3$^+$ cells were present within the GCs at day 10, despite being abundant in the T cell area. Collectively, these results indicated that the T_{FR} cells failed to develop during the peak of the influenza infection, but accumulated in the mLN at later time points.

Previous studies have shown that T_{FR} cells develop quickly (days 7–14) upon immunization with soluble antigens[20,21,23]. To test whether the delayed appearance of T_{FR} cells was unique to influenza, we enumerated T_{FR} cells in B6 mice that were either immunized with influenza hemagglutinin (HA) adsorbed to alum (Supplementary Fig.1 d,e) or infected with LCMV-Armstrong (Supplementary Fig. 1 f,g). In agreement with the published studies, we found that T_{FR} cells were readily detected at day 9 after HA immunization and were maintained for at least 30 days (Supplementary Fig. 1 d,e). By contrast, T_{FR} cells were virtually undetectable at day 9 following LCMV-Armstrong infection, but accumulated in large numbers at day 30 after infection (Supplementary Fig. 1 f,g). Collectively, these results suggested that, whereas T_{FR} cell responses quickly develop following soluble protein immunization, T_{FR} cells fail to differentiate at the peak of acute viral infections.

T_{FR} cells exhibit low expression of CD25

T_{FR} cells depend on Bcl-6[20–22], whose expression is inhibited by IL-2[10,14,16]. To examine the relationship between T_{FR} cells and IL-2 signaling, we divided the CD69$^+$Foxp3$^+$CD4$^+$ T-cell population into CD25^{hi} and CD25^{lo} cells and analyzed the expression of T_{FR} cell markers in these subpopulations (Fig. 2a,c). We found that CD25^{lo}Foxp3$^+$ cells, but not CD25^{hi}Foxp3$^+$ cells, up-regulated T_{FR} markers following infection (Fig. 2a,c). Importantly, although CD25^{lo}Foxp3$^+$ cells were present at the peak of the infection (d10), they expressed low amount of CXCR5, Bcl-6 and PD-1 relative to later time points, suggesting that lack of

T_{FR} cells at the peak of the infection was not due to a lack of $CD25^{lo}Foxp3^{+}$ cells (Supplementary Fig. 2a–c). Similar results were obtained in LCMV-infected mice or HA-Alum-immunized mice (Supplementary Fig. 2d,e). Thus, unlike conventional T_{reg} cells, which are $CD25^{hi}$, T_{FR} cells are $CD25^{lo}$.

We next evaluated STAT5 phosphorylation in T_{FR} and conventional T_{reg} cells and found that pSTAT5 was reduced in T_{FR} cells compared to conventional T_{reg} cells (Fig. 2d), suggesting that T_{FR} and conventional T_{reg} cells responded differently to IL-2. To confirm this conclusion, we sorted conventional T_{reg} cells ($Foxp3^{+}CD69^{hi}PD\text{-}1^{lo}CXCR5^{lo}CD25^{hi}$) and T_{FR} cells ($Foxp3^{+}CD69^{hi}PD\text{-}1^{hi}CXCR5^{hi}CD25^{lo}$) from the mLN of day 30 infected B6.Foxp3–DTR–GFP mice and performed RNA-sequencing (RNA-seq) and Gene Set Enrichment Analysis (GSEA) to identify hallmark-signaling pathways differentially enriched in these populations (Fig. 2e,f). Approximately 2,000 genes were differentially expressed between conventional T_{reg} and T_{FR} cells (Supplementary Table 1). Importantly, the IL-2–STAT5 signaling pathway had the highest normalized enrichment score (NES=3.54; FDR < 0.001) and contained the largest number of genes up-regulated in T_{reg} cells relative to T_{FR} cells (Fig. 2e). Of the 200 genes in the hallmark IL-2–STAT5 signaling pathway, 72 were significantly downregulated in T_{FR} vs T_{reg} cells (Fig. 2f and Supplementary Tables 2,3). Interestingly, despite their low expression of CD25 (Fig. 2g), T_{FR} cells expressed high amounts of IL-2Rβ (CD122) (Fig. 2h), suggesting that T_{FR} cells may have some remaining capacity to respond to IL-2, particularly when its physiological concentration is sufficiently high[27]. Altogether, our results indicated that the IL-2–STAT5 signaling pathway was downregulated in T_{FR} cells compare to conventional T_{reg} cells.

$CD25^{+}$ T_{reg} cells are the precursors of T_{FR} cells

Previous studies showed that T_{FR} cells differentiate from pre-existing $Foxp3^{+}$ T_{reg} precursors[20,21]. Given that T_{FR} cells were $CD25^{lo}$, we used adoptive-transfer experiments to test whether T_{FR} cells were derived from pre-existing $CD25^{hi}Foxp3^{+}$ or $CD25^{lo}Foxp3^{+}$ T cells. Therefore, we sorted $CD25^{hi}Foxp3^{+}$ or $CD25^{lo}Foxp3^{+}$ $CD4^{+}$ T cells from the spleen of naïve B6.Foxp3–DTR–GFP ($CD45.2^{+}$) mice, which express the diphtheria-toxin receptor and the eGFP genes under the control of the Foxp3 promoter, and adoptively transferred equivalent numbers of these cells into naïve *Tcrb*$^{-/-}$ *Tcrd*$^{-/-}$ mice, that lack T cells. We also transferred total $CD8^{+}$ and $CD4^{+}$ T cells from B6.CD45.1 mice to provide a competent T-cell environment. One day later, mice were infected with influenza and the donor-derived $Foxp3^{+}$ cells were characterized on day 30. The frequencies and numbers of activated $Foxp3^{+}$ cells derived from the $CD45.2^{+}$ donors were increased in recipients of $CD25^{hi}Foxp3^{+}$ cells compared to recipients of $CD25^{lo}Foxp3^{+}$ cells (Fig. 3a,b). We also found that nearly 6% of the progeny derived from $CD25^{hi}Foxp3^{+}$ cells up-regulated Bcl-6 and CXCR5, whereas few of the progeny derived from $CD25^{lo}Foxp3^{+}$ cells up-regulated Bcl-6 and CXCR5 (Fig. 3c). As a result, the numbers of $CD45.2^{+}$ T_{FR} cells were significantly higher in recipients of $CD25^{hi}Foxp3^{+}$ cells compared to recipients of $CD25^{lo}Foxp3^{+}$ cells (Fig. 3d). Importantly, the number of $CD45.1^{+}Foxp3^{+}$ cells, and the number of $CD45.1^{+}$ T_{FR} cells were similar in the two groups (Fig. 3e,f). These data indicated that pre-existing $CD25^{hi}Foxp3^{+}$ cells, but not pre-existing $CD25^{lo}Foxp3^{+}$ cells, differentiate into T_{FR} cells following influenza infection.

Recent data suggest that T_{FR} cells can also be derived from $CD4^+Foxp3^-$ precursors[28]. Therefore, we performed adoptive-transfer experiments to compare the capacity of $CD4^+Foxp3^-$ and $CD25^{hi}Foxp3^+$ cells to differentiate into T_{FR} cells following infection. Although some $CD4^+Foxp3^-$ cells up-regulated Foxp3 after infection (data not shown), $CD45.2^+$ T_{FR} cells were only generated from $CD25^{hi}Foxp3^+$ cell precursors (Fig. 3g,h). Collectively, these data indicated that $CD25^{hi}Foxp3^+$ cells are the precursors of T_{FR} cells after influenza infection.

We next tested whether the $Foxp3^+$ cells derived from the $CD25^{hi}Foxp3^+$ donors maintained CD25 expression (Fig. 3i). We found that, although the majority of $Foxp3^+$ progeny derived from the $CD25^{hi}Foxp3^+$ donors were $CD25^{hi}$, some cells lost expression of CD25 and only the $CD25^{lo}$ cells up-regulated T_{FR} markers (Fig. 3i). Collectively, these results demonstrated that a fraction of the activated $CD25^+Foxp3^+CD4^+$ T cells down-regulate CD25 and up-regulate Bcl-6, PD-1 and CXCR5 late after infection.

IL-2 signaling precludes T_{FR} cell development

Given that IL-2 signaling inhibits Bcl-6 expression[10,14,16], we next tested whether T_{FR} cells could develop in a high-IL-2 environment. To do this, B6 mice were infected with influenza, treated them with either 30,000 units (U) of recombinant IL-2 (rIL-2) or PBS for nine consecutive days starting on day 20 and T_{FR} cells were enumerated in the mLN on day 30. As a control, we analyzed day 10 infected mice. As expected, the frequencies and numbers of T_{FR} cells were higher in day 30 infected mice relative to day 10 infected mice (Fig. 4a,b). By contrast, T_{FR} cells failed to accumulate in rIL-2-treated mice (Fig. 4a,b), suggesting that a high-IL-2 environment prevented the accumulation of T_{FR} cells.

We next determined the kinetic of IL-2 production during influenza infection using *Il21*-mCherry-*Il2*-emGFP dual reporter transgenic mice[29] (Fig. 4c). We found that the frequency of IL-2-producing $CD4^+$ T cells peaked at day 10 and declined thereafter (Fig. 4c). We also found that the frequency of IL-2-producing $CD4^+$ T cells was significantly increased in day 10 influenza-infected mice relative to day 10 HA-immunized mice (Supplementary Fig. 3). Given that IL-2 is highly produced at the peak of the infection, we hypothesized that strong IL-2 signals prevented the differentiation of T_{FR} cells at this time. To address this possibility, we infected B6 mice with influenza, treated them daily from day 3 to day 9 with neutralizing IL-2 antibodies (JES6-1A12 + S4B6-1) or control antibody (2A3), and analyzed the Foxp3 compartment in the mLN on day 10 (Fig. 4d,e). As expected, we detected very few T_{FR} cells in control-treated mice. The frequency and number of T_{FR} cells was, however, significantly increased in the anti-IL-2–treated mice (Fig. 4d,e). These results suggested that an elevated concentration of IL-2 at the peak of the infection prevented Foxp3-expressing cells from differentiating into T_{FR} cells. We also found more T_{FH} cells, but less conventional $CD25^+$ T_{reg} cells in the anti-IL-2-treated mice compared to control mice (Fig. 4f–h), which is consistent with previous studies showing that IL-2 signaling is required for $CD25^{hi}Foxp3^+$ T_{reg} cell expansion[2,7,30–32], but prevents T_{FH} cell differentiation[14–16,26].

To confirm that IL-2 signaling inhibited T_{FR} cell differentiation, we sorted $CD25^{hi}Foxp3^+$ cells from day 7 influenza-infected B6.Foxp3-DTR–GFP mice, activated them *in vitro* with anti-CD3 and anti-CD28 beads in the presence of high (200U/ml) or low (5U/ml) rIL-2

concentrations and assessed the phenotype of Foxp3$^+$ cells three days later (Fig. 4i–o). Foxp3$^+$ cells activated in the presence of high-IL-2 concentrations expressed high levels of CD25, Blimp-1 and T-bet relative to Foxp3$^+$ cells cultured in low-IL-2 conditions (Fig. 4i–k). In contrast, Bcl-6 and CXCR5 were up-regulated in Foxp3$^+$ cells cultured in low-IL-2 concentrations (Fig. 4l,m). As a result, Bcl-6^{hi}CXCR5^{hi} cells differentiated in the low but not high-IL-2 cultures (Fig. 4n,o). Collectively, our data indicated that, while elevated IL-2 signaling at the peak of the infection promoted CD25^{hi} T_{reg} cell responses, it simultaneously prevented Foxp3-expressing cells from up-regulating Bcl-6 and CXCR5 and differentiating into T_{FR} cells.

IL-2 prevents T_{FR} cell responses by promoting Blimp-1

IL-2 inhibits Bcl-6 expression by up-regulating Blimp-1[14,15] and by favoring the formation of T-bet–Bcl-6 complexes, which mask the Bcl-6 DNA-binding domain and prevent it from binding to its target genes[26]. Thus, we next assessed the expression of these transcription factors in Foxp3$^+$ cells following influenza infection (Fig. 5a–c). To do this, B6.Blimp-1–YFP reporter mice were infected and the expression of the Blimp-1–YFP reporter was examined in CD69$^+$Foxp3$^+$CD4$^+$ T cells (Fig. 5a,b). We found that nearly 12% of these cells were Blimp-1–YFP$^+$ (Fig. 5a). As predicted, Blimp-1–YFP$^+$ cells were Bcl-6^{lo} (Fig. 5a). We also found that although some Blimp-1–YFP$^+$ cells were CD25$^{int/low}$, the majority of Blimp-1–YFP$^+$ cells expressed high amounts of CD25 (Fig. 5b). We next analyzed T-bet expression and found that it was highly expressed in CD25^{hi}Blimp-1$^+$ cells relative to CD25^{lo}Blimp-1$^-$ cells (Fig. 5c). Thus, in agreement with previous studies[33–35], T_{reg} cells expressed T-bet and Blimp-1 following influenza infection.

To investigate the role of these transcription factors in T_{FR} cell development, we made mixed-bone marrow (BM) chimeras in which irradiated *Tcrb*$^{-/-}$*Tcrd*$^{-/-}$ recipient mice were reconstituted with a 50:50 mixture of BM obtained from CD45.1$^+$ wild-type and CD45.2$^+$ *Tbx21*$^{-/-}$ (T-bet-deficient) B6 donor mice. Two months later, chimeras were infected with influenza and the frequency of T_{FR} cells derived from each donor was determined on day 10. As expected, we failed to detect Bcl-6^{hi}CXCR5^{hi} cells within the CD25^{hi}Foxp3$^+$ compartment of either donor (Fig. 5d). Although we did observe approximately 5% Bcl-6^{hi}CXCR5^{hi} cells in the CD25^{lo}Foxp3$^+$ compartment, there was no difference between the wild-type and *Tbx21*$^{-/-}$ donor cells (Fig. 5d). These results suggested that T-bet did not prevent T_{FR} cell differentiation at the peak of the infection.

To address a potential role for Blimp-1 in preventing T_{FR} differentiation, we generated mixed-BM chimeras using wild-type (CD45.1$^+$) and *Prdm1*$^{fl/fl}$-*Lck*-$^{cre/+}$ (CD45.2$^+$) donors (WT–*Prdm1*$^{-/-}$ chimeras). After reconstitution, chimeras were infected with PR8 and analyzed at day 10. As expected, very few wild-type CD25^{lo}Foxp3$^+$ cells expressed T_{FR} markers at day 10 post-infection. However, 20% of the *Prdm1*$^{-/-}$CD25^{lo}Foxp3$^+$ cells were T_{FR} cells (Fig. 5e). These results suggested that Blimp-1 prevented the development of T_{FR} cells at the peak of the influenza infection.

Finally, we examined whether IL-2 prevents T_{FR} cell differentiation by a Blimp-1-dependent mechanism. Thus, WT–*Prdm1*$^{-/-}$ chimeras were infected with influenza, treated daily with rIL-2 or control PBS starting at day 20, and the T_{FR} cell response was assessed within the

wild-type and *Prdm1*$^{-/-}$ compartments on day 30 after infection (Fig. 5f,g). Similar to our prior experiment, we found more CD25^{lo}Foxp3^{+} cells with a T_{FR} cell phenotype in the *Prdm1*$^{-/-}$ compartment relative to the wild-type compartment in the PBS-treated mice (Fig. 5f). We also found diminished frequencies of T_{FR} cells in the wild-type compartment of the rIL-2 treated mice relative to PBS-treated mice (Fig. 5f). However, we observed similar frequencies of *Prdm1*$^{-/-}$ T_{FR} cells in both PBS control and IL-2-treated mice (Fig. 5f). As a consequence, the ratio of *Prdm1*$^{-/-}$ to wild-type T_{FR} cells was increased in the rIL-2-treated mice compared to PBS control counterparts (Fig. 5g). These results indicated that high-IL-2 signaling directly prevented T_{FR} cell differentiation by an intrinsic IL-2/Blimp-1-dependent mechanism.

T_{FR} cells maintain B-cell tolerance after infection

We next used three independent approaches to test the effect of T_{FR} cells on the B cell response to influenza. First, we crossed Bcl-6$^{fl/fl}$ mice[36] to Foxp3$^{YFP/Cre}$ mice[37] to generate Bcl-6$^{fl/fl}$Foxp3$^{YFP/Cre}$ mice, in which the zinc finger-domains of Bcl-6 are conditionally deleted in Foxp3–expressing T cells[36]. Bcl-6$^{fl/fl}$Foxp3$^{YFP/Cre}$ mice were infected with influenza and analyzed them on day 30. As expected, the number of T_{FR} cells was reduced in Bcl-6$^{fl/fl}$Foxp3$^{YFP/Cre}$ mice compared to control mice (Fig. 6a,b). In contrast, T_{FH} cells normally accumulated in Bcl-6$^{fl/fl}$Foxp3$^{YFP/Cre}$ mice (Fig. 6c,d). Similar results were obtained when we used fluorochrome-labeled MHC Class II tetramers to identify influenza nucleoprotein (NP)-specific T_{FH} cells (Supplementary Fig. 4a,b). We also found GC B cells normally accumulated in control and Bcl-6$^{fl/fl}$Foxp3$^{YFP/Cre}$ mice (Fig. 6e,f). Importantly, however, the frequency and number of CD138^{+} antibody-secreting cells (ASCs) were increased in Bcl-6$^{fl/fl}$Foxp3$^{YFP/Cre}$ mice relative to control mice (Fig. 6g,h). These results suggested that lack of T_{FR} cells did not change T_{FH} cell or the GC B-cell responses, but promoted the accumulation of CD138^{+} ASCs.

To confirm this observation, we generated BM chimeras in which T_{FR} cells were selectively depleted after diphtheria toxin (DT) administration (Fig. 7a–f). Thus, we reconstituted irradiated *Tcrb*$^{-/-}$*Tcrd*$^{-/-}$ recipient mice with a 50:50 mix of *Cxcr5*$^{-/-}$and Foxp3-DTR BM (Foxp3-*Cxcr5*$^{-/-}$ chimeras), or wild-type BM and Foxp3-DTR BM (Foxp3-WT chimeras). Because T_{FR} cells cannot be produced from *Cxcr5*$^{-/-}$ precursors[20], all the T_{FR} cells in the influenza-infected Foxp3-*Cxcr5*$^{-/-}$ chimeras developed from the Foxp3-DTR donors (Fig. 7a). In contrast, T_{FR} cells in the Foxp3-WT chimeras developed equally from the WT and Foxp3-DTR donors (Fig. 7a). As a consequence, T_{FR} cells were depleted following DT administration in the Foxp3-*Cxcr5*$^{-/-}$ but not in the Foxp3-WT influenza-infected chimeras (Fig. 7b,c). The T_{reg} cell response was, however, similar in the two groups (Fig. 7d). Therefore, we infected the chimeric mice with influenza, treated them with DT every four days starting on day 15 and enumerated T_{FH} cells, GC B cells and CD138^{+} ASCs on day 50 in the mLN. We found similar frequencies and numbers of T_{FH} cells and GC B cells (Supplementary Fig. 5a–d) in the DT-treated Foxp3-*Cxcr5*$^{-/-}$ and Foxp3-WT chimeras. However, CD138^{+}ASCs accumulated to a greater frequency in Foxp3-*Cxcr5*$^{-/-}$ chimeras compared to Foxp3-WT controls (Fig. 7e,f). Importantly, no differences were detected between PBS-treated Foxp3-*Cxcr5*$^{-/-}$and Foxp3-WT chimeras (Supplementary Fig. 5e). These findings indicated that lack of T_{FR} cells promotes the expansion of CD138^{+}ASCs.

To confirm our observations, we treated influenza-infected B6 mice daily with 15,000U of rIL-2 starting on day 20 to deplete T_{FR} cells, and evaluated the - cell response in the mLN on day 30. T_{FR} cells were significantly depleted in rIL-2-treated mice (Supplementary Figure 5f). In contrast, rIL-2 treatment did not affect the accumulation of total or NP-specific T_{FH} cells at this time and dosage (Supplementary Fig. 5g–j). Similarly, the GC B cell response was similar in PBS and rIL-2 treated mice (Supplementary Fig. 5k,l). In contrast, the frequencies and numbers of $CD138^+$ASCs were increased in rIL-2-treated mice (Fig. 7g,h). Collectively, our data indicated that absence of T_{FR} cells late after infection promoted the expansion of $CD138^+$ASCs.

Lack of T_{FR} cell promotes the outgrowth of self-reactive B cell clones following immunization with T-dependent antigens[21]. To characterize the role of T_{FR} cells in controlling the influenza-specific B-cell response, we used fluorochrome-labeled recombinant NP-tetramers[10,16] to identify NP-specific B cells in IL-2-treated and Bcl-$6^{fl/fl}$Foxp$3^{YFP/Cre}$ mice (Fig. 8a–h). The frequencies and numbers of NP-specific GC B cells were similar in control and rIL-2 treated mice (Fig. 8a,b). In contrast, while 30% of the $CD138^+$ ASCs were NP-specific in control mice, only 8% of the $CD138^+$ ASCs were NP-specific in the rIL-2-treated mice (Fig. 8c). As a consequence, the number of NP-specific $CD138^+$ ASCs was similar in control and rIL-2 treated mice (Fig. 8d). Similar results were obtained when comparing Bcl-$6^{fl/fl}$Foxp$3^{YFP/Cre}$ and control counterparts (Fig. 8e,f). Finally, the titers of influenza-specific serum IgG were similar in PBS and rIL-2-treated mice (Fig. 8g), or when we compared the serum from Bcl-$6^{fl/fl}$Foxp$3^{YFP/Cre}$ and control mice (Fig. 8h). These results suggested that a lack of T_{FR} cells did not significantly affect the influenza-specific B-cell response, but instead promoted the accumulation of non-influenza-specific $CD138^+$ ASCs.

We next hypothesized that these ASCs represented the differentiated daughter cells of self-reactive B cells that are known to be generated in the GCs during infections[38]. To test this possibility, we first enumerated histone-specific, IgG-secreting cells by ELISPOT in the mLNs of day 30-infected PBS and rIL-2-treated mice. As expected, we found very few histone-specific ASCc in the mLN of PBS-treated mice (Fig. 8i). In contrast, the frequency of anti-histone, IgG ASCs was increased in rIL-2-treated mice, suggesting that lack of T_{FR} cells resulted in the development of anti-nuclear antibody (ANA) responses (Fig. 8i). Thus, we evaluated the serum samples for ANA reactivity. As expected, PBS-treated control mice lacked ANAs, whereas IL-2-treated mice were ANA positive (Fig. 8j). Finally, we evaluated the presence of ANAs in the serum of Bcl-$6^{fl/fl}$Foxp$3^{YFP/Cre}$ mice. We found that, while the sera from B6 infected mice (Fig. 8k) or naïve Bcl-$6^{fl/fl}$Foxp$3^{YFP/Cre}$ mice (Supplementary Fig. 6) were negative for ANA staining, the sera obtained from day 30-infected Bcl-$6^{fl/fl}$Foxp$3^{YFP/Cre}$ mice were positive (Fig. 8k). Therefore, our data indicated that T_{FR} cells prevented the expansion of self-reactive ASCs after influenza infection.

DISCUSSION

We show here that T_{FR} cells are characterized by low expression of CD25 and that IL-2 signaling inhibits, rather than promotes, the development of T_{FR} cells. Correspondently, T_{FR} cells fail to accumulate at the peak of the influenza infection, a time during which IL-2 is

highly produced. However, after IL-2 withdrawal, some Foxp3$^+$ cells down-regulate CD25, up-regulate Bcl-6, express CXCR5 and differentiate into T_{FR} cells, which migrate into the B-cell follicles to prevent self-reactive B-cell responses. Thus, unlike conventional T_{reg} cells, high-IL-2 signaling precludes T_{FR} cell development. Importantly, IL-2 consumption by CD25$^+$ T_{reg} cells is required for the initial development of virus-specific T_{FH} cells[10]. Thus, IL-2-consumption acts as a rheostat that, while facilitating virus-specific T_{FH} cell responses, it selectively prevents T_{FR} cell development at the peak of the infection.

T_{FR} cells prevented self-reactive ASCs, but had no significant effect on the influenza-specific B-cell response, suggesting that T_{FR} cells may be self-specific rather than influenza-specific. This idea is consistent with data showing that the TCR repertoire of T_{FR} cells is skewed towards self-antigens[39], and so is the TCR repertoire of thymic-T_{reg} cells[40,41], which we show here are the likely precursors of T_{FR} cells after influenza infection. However, T_{FR} cells prevent antigen-specific B-cell responses following immunization with soluble antigens, suggesting that antigen-specific T_{FR} cells can develop under some circumstances [20,21,23,28]. In this regard, a recent study suggests that a fraction of the T_{FR} cells differentiate from naïve T-cells precursors following immunization and are specific for the immunizing Ag[28]. Thus, depending on the specific nature of the immune response, T_{FR} cells can prevent foreign and self-reactive B-cell responses based on their origin and TCR-specificity. In any case, the capacity of T_{FR} cells to prevent influenza-specific effector B responses is overcome in the context of influenza infection. Indeed, influenza-NP is normally complexed with viral-RNA[42], which targets it to the intracellular TLR7 compartment following BCR stimulation[43]. Thus, it is possible that co-ligation of the BCR and pathogen-recognition-receptors in virus-specific B cells synergize to overcome T_{FR}-mediated suppression during influenza infection.

We found that Blimp-1, but not T-bet, suppresses T_{FR} cell development. However, we failed to detect Bcl-6 up-regulation in CD25^{hi} T_{reg} cells even in Blimp-1-deficient cells, suggesting that Bcl-6 expression in CD25^{hi} cells is prevented by additional Blimp-1-independent mechanisms. Given that STAT5 binds to the *Bcl-6* promoter and directly represses Bcl-6 expression in response to high-IL-2 signaling[26,44–46], it is likely that strong IL-2 signaling through CD25 prevents Bcl-6 expression by a direct STAT5-dependent mechanism.

Our data showing that IL-2 prevents T_{FR} cell responses are in conflict with the notion that IL-2–STAT5 signaling is required for maintaining Foxp3 expression[1]. However, T_{FR} cells express high amounts of CD122. Thus, although insufficient for inducing sustained Blimp-1 expression in low-IL-2 environments, basal IL-2–STAT5 signaling through the intermediate-affinity IL-2R may be sufficient to prevent Foxp3 down-regulation in T_{FR} cells. Alternatively, T_{FR} cell homeostasis may be partially independent of IL-2, but may require signals from other common–γ chain cytokines and costimulatory molecules, such as IL-7, IL-15 or ICOS which can contribute towards the maintenance of Foxp3-expressing cells in the absence of IL-2[18,19,47,48]. In any case, it is likely that conventional CD25$^+$ T_{reg} and T_{FR} cells use different cellular and molecular pathways for their homeostatic maintenance.

In summary, our data demonstrate that IL-2 signaling temporarily inhibits T_{FR} cell responses during influenza infection. However, once the immune response is resolved, T_{FR} cells

differentiate and home to B cell follicles, where are required for maintaining B cell tolerance after infection. Thus, the same mechanism that promotes conventional T_{reg} cell responses, namely IL-2 signaling, also prevents T_{FR} cell formation. Collectively, our data provide a new perspective into how IL-2 dynamically regulates T_{reg} cell homeostasis and function along the course of a relevant pathogen infection.

METHODS

Mice

C57BL/6 (B6), B6.SJL-*Ptprca Pepcb*/BoyJ (B6.CD45.1), B6.129S6-*Tbx21tm1Glm*/J, (B6.*Tbx21*$^{-/-}$) B6.129P2-*Tcrβ*^{tm1Mom} *Tcrδ*^{tm1Mom} (*Tcrb*$^{-/-}$ *Tcrd*$^{-/-}$), B6.129S6-*Sh2d1atm1Pls*/J (*Sh2d1a*$^{-/-}$), B6.129-Prdm1tm1Clme/J (*Prdm1*$^{fl/fl}$ and B6.Cg-Tg(Lck-cre)3779Nik/J, B6.129S(FVB)-*Bcl-6tm1.1Dent*/J (*Bcl-6*$^{fl/fl}$, B6.129(Cg)-*Foxp3tm4(YFP/icre)Ayr*/J (Foxp3$^{YFP\text{-}/Cre}$), B6.129S2(Cg)-Cxcr5^{tm1Lipp}/J (*Cxcr5*$^{-/-}$) were originally obtained from Jackson Laboratories. *Il21*-mCherry-*Il2*-emGFP dual-reporter transgenic mice were obtained from W. J. Leonard (NHLBI). Blimp-1 reporter mice were obtained from E. Meffre (Yale University). B6.129S6-*Foxp3*^{tm1DTR} (Foxp3–DTR–GFP) mice were originally obtained from A Rudensky (Memorial Sloan-Kettering Cancer Center). *Prdm1*$^{fl/fl}$ mice were crossed to B6.Cg-Tg(Lck-cre)3779Nik/J mice to generate B6.*Prdm1*$^{fl/fl}$-*Lck*$^{cre/+}$ mice. *Bcl-6*$^{fl/fl}$ mice were crossed to *Foxp3*$^{YFP\text{-}/Cre}$ mice to generate *Bcl-6*$^{fl/fl}$Foxp3$^{YFP/Cre}$ mice. All mice were bred in the University of Alabama at Birmingham (UAB) animal facility. All experimental procedures involving animals were approved by the UAB Institutional Animal Care and Use Committee and were performed according to guidelines outlined by the National Research Council.

Infections, BM chimeras and *in vivo* treatments

Influenza virus infections were performed intranasally (i.n) with 6,500 VFU of A/PR8/34 (PR8) in 100 μl of PBS. Acute LCMV infections were established by intraperitoneal injection with 2×10^5 PFU LCMV-Armstrong. In some experiments mice were immunized with 50 μg of recombinant hemagglutinin (HA) adsorbed to Alum (Imject® Alum, Thermo Scientific™). BM chimeric mice were generated by irradiating the indicated recipient mice with 950 Rads from an X-ray source delivered in 2 equal doses administered 4–5 h apart. Following irradiation, mice were intravenously injected with 5 × 106 total BM cells and were allowed to reconstitute for 8–10 weeks before influenza infection. In indicated experiments, experimental animals received an intraperitoneal injection of 50 μg/kg of diphtheria toxin (DT - Sigma) at the indicated time points. In some experiments, mice were intraperitoneally administered recombinant IL-2 (National Cancer Institute) at the indicated time points. Control mice received injections of PBS. In some experiments mice were treated with 500 μg of a mix of anti-IL-2 neutralizing antibodies (JES6-1A12 and S4B6) or 500 μg of Isotype control (2A3), all obtained from BioXcell.

Immunofluorescence

Lymph nodes were frozen in OCT (Tissue-Tek; Sakura) and 7 μm frozen sections were prepared and stained as described [49]. Slides were probed for 30 min at 25 °C with anti-IgD^b (2170-170), Anti-B220 (RA3-6B2) and anti-CD35 (8C12) obtained from BD Biosciences,

and anti-Foxp3 (MF-14) from BioLegend. Biotin-conjugated primary antibodies were detected with streptavidin–Alexa Fluor 555 (S21381; Invitrogen Life Sciences). Images were obtained using a Zeiss Axioplan 2 microscope with a Zeiss Axiocam digital camera (Zeiss).

Cell preparation and flow cytometry

Cell suspensions from mLNs were prepared and filtered through a 70 μm nylon cell strainer (BD Biosciences). Cells were washed and resuspended in PBS with 2% donor calf serum and 10 μg/ml FcBlock (2.4G2 -BioXCell) for 10 min on ice before staining with fluorochrome-conjugated antibodies. Fluorochrome-labeled anti-CD45.1 (clone A20, dilution 1/400), anti-CD45.2 (clone 104, dilution 1/400), anti-CD19 (clone 1D3, dilution 1/200), anti-CD138 (clone 281.2, dilution 1/500), Anti-Bcl-6 (clone K112.91, dilution 1/50), anti-CXCR5 (clone 2G-8, dilution 1/50), anti-CD4 (clone RM4–5, dilution 1/200), anti-CD95 (clone Jo2 dilution 1/500), anti-CD69 (clone H1.2F3, dilution 1/200), anti-GL7 (clone, GL7, dilution 1/500), anti-CD25 (clone PC61, dilution 1/200), anti-Blimp-1 (clone 5E7, dilution 1/100) and anti-pSTAT5 (PY694, clone 47-BD, dilution 1/50) were obtained from BD Biosciences. Anti-PD-1 (clone J43, dilution 1/100) and anti-Foxp3 (clone FJK-16s, dilution 1/200) were purchased from eBioscience. Anti-T-bet (clone 4B10, dilution 1/200) was purchased from BioLegend. Recombinant influenza nucleoprotein (NP) B-cell tetramers were prepared as previously described [16]. The I-A^b NP311–325 MHC class II tetramer was obtained from the NIH Tetramer Core Facility. Dead cell exclusion was performed using 7-AAD (BioLegend). Intracellular staining was performed using the mouse regulatory T cell staining kit (eBioscience) following manufacturer's instructions. For p-STAT5 staining, cells were stimulated with 100 ng/ml of rIL-2 for 15 minutes and then fixed and permeabilized with BD Cytofix/cytoperm^{TM} buffer (BD) and the Phosflow Perm Buffer III (BD) following the manufacturer's instructions. Flow cytometry was performed using a FACSCanto II (BD Biosciences) and an Attune NxT Flow Cytometer (ThermoFischer Scientific).

Cell purification and adoptive transfer

$CD45.1^+$ $CD4^+$ and $CD45.1^+$ $CD8^+$ T cells were purified from the spleens of naïve B6.$CD45.1^+$ mice by positive selection with anti-CD4 and anti-CD8 MACS beads (Miltenyi Biotec). $CD4^+Foxp3^+CD25^{hi}$, $CD4^+Foxp3^+CD25^{lo}$ and $CD4^+Foxp3^-$ T cells were sorted from spleens of Foxp3-DTR/GFP mice using a FACSAria (BD Biosciences) after positive selection with anti-CD4 MACS beads. Sorted cells (5×10^5) were transferred intravenously into naïve *Tcrb*$^{-/-}$ *Tcrd*$^{-/-}$ recipient mice. All sorted T-cell subsets were more than 95% pure.

In vitro stimulation of influenza-induced T_{reg} cells

$CD4^+Foxp3^+CD25^{hi}$ cells were sorted from spleens and mLNs of influenza-infected B6.129S6-*Foxp3*^{tm1DTR} mice using a FACSAria (BD Biosciences) after positive selection with anti-CD4 MACS beads. Sorted cells were activated using pre-load anti-CD3/CD28 MACSiBead Particles (T_{reg} Expansion Kit, Miltenyi Biotec) at a bead-to-cell ratio of 3:1 in the presence of the indicated concentration of rIL-2 (Peprotech). Cells were cultured for 72 h at 37 °C in 125 μl in round-bottomed 96-well plates in RPMI-1640 supplemented with sodium pyruvate, HEPES (pH 7.2–7.6 range), nonessential amino acids, penicillin, streptomycin, 2-mercaptoethanol and 10% heat-inactivated FCS (all from Gibco).

ELISAs

96-well plates (Corning™ Clear Polystyrene 96-Well Microplates) were coated overnight with purified PR8 proteins [50] at 1 μg/ml in 0.05 M Na_2CO_3 pH 9.6. Coated plates were then blocked for 1 h with 1% BSA in PBS. Serum from PR8-infected mice was collected and serially diluted (3-fold) in PBS with 10 mg/ml BSA and 0.1% Tween 20 before incubation on coated plates. After washing, bound antibody was detected with HRP-conjugated goat Anti-Mouse, IgG (g heavy chain specific) Ab (Southern Biotech) and quantified by spectrophotometry at 405 nm (OD).

ELISPOT

Multiscreen cellulose filter plates (Millipore) were coated overnight with 10 μg of histone from calf thymus (Sigma-Aldrich). Cells from the mLN were collected and plated starting at 3×10^6/well and in 2-fold serial dilutions in complete RPMI 1640 containing 10% FBS. After 5 h, the wells were washed with PBS containing 0.5% BSA and 0.05% Tween 20, and IgG was detected using alkaline phosphatase-conjugated goat anti-mouse IgG (Jackson immunoresearch). Spots were counted using a dissecting microscope. Images were taken using a CTL-immunoSpot S5 analyzer.

ANA analysis

For ANA analysis, serum was diluted 1:5 in PBS/0.2% BSA and incubated on Kallestad® HEp-2 Slides (Bio-rad). Slides were washed and stained with anti–mouse IgG FITC (SouthernBiotech). Slides were mounted with Aqua PolyMount and analyzed on a fluorescent microscope (Axio Observer.Z1). Images were obtained using a Zeiss Axioplan 2 microscope with a Zeiss Axiocam digital camera (Zeiss).

RNA-sequencing (RNA-seq)

Conventional T_{reg} cells ($CD19^-CD4^+Foxp3^+CD69^{hi}PD\text{-}1^{lo}CXCR5^{lo}CD25^{hi}$) and T cells T_{FR} cells ($CD19^-CD4^+Foxp3^+CD69^{hi}PD\text{-}1^{hi}CXCR5^{hi}CD25^{lo}$) were sorted from the mLN of Foxp3-DTR/GFP mice at day 30 after influenza infection using a FACSAria (BD Biosciences) after positive selection with anti-CD4 MACS beads (Miltenyi Biotec). RNA was isolated from the sorted cells using the Single cell RNA purification kit (Norgen Biotek Corp). Three replicates from three independent experiments for each condition were analyzed with RNA-seq. Library preparation and RNA sequencing was conducted through Genewiz. Libraries were sequenced using a 1×50bp single end rapid run on the HiSeq2500 platform. Sequence reads were trimmed to remove possible adapter sequences and nucleotides with poor quality (error rate < 0.05) at the end. After trimming, sequence reads shorter than 30 nucleotides were discarded. Remaining sequence reads were mapped to the *Mus musculus* mm10 reference genome using CLC genomics workbench v. 9.0.1 Differential gene expression was determined using DESeq2. Genes with an adjusted *P*-value <0.05 and an absolute Log_2-fold change > 1 were considered significantly differentially expressed genes between conventional T_{reg} cells and T_{FR} cells.

GSEA, hierarchical clustering and visualization of RNA sequencing results

GSEA was performed using the Molecular Signatures Database on the publically available MIT BROAD Institute server. We ranked the 2002 genes obtained from RNA sequencing (Genewiz) according to a logarithmic transformation of each gene's *P*-value multiplied by the sign of the corresponding logarithmic fold change, and subsequently utilized these rank lists to perform a gene set enrichment analysis (Broad Institute's GSEA Java app, version 2.2.4). Given gene sets can include both activated and repressed genes, we additionally performed an extended assessment of gene enrichment of the two complementary gene sets against N ranked genes[51, 52], to confirm the original GSEA results. Separately, we performed hierarchical clustering analysis [53, 54] of IL-2-induced genes that are differentially expressed in T_{reg} cells vs T_{FR} cells, using Matlab (version R2016b). Differential clusters are presented in the form of an annotated heatmap based on standardized expression values, along with the resulting hierarchical clustering dendogram. We additionally plotted in Matlab (version R2016b) the number and proportion of genes expressed within hallmark sets (GSEA), and their corresponding p-values.

Statistical analysis

GraphPad Prism software (Version 5.0a) was used for data analysis. The statistical significance of differences in mean values was determined using a two-tailed Student's *t*-test. *P* values of less than 0.05 were considered statistically significant.

Data availability

The data that support the findings of this study are available from the corresponding author upon request. RNA-seq data are available from GEO under accession code GSE101016.

Supplementary Material

Refer to Web version on PubMed Central for supplementary material.

Acknowledgments

The authors would like to thank W. J. Leonard (US National Institutes of Health) for providing the *Il21*-mCherry-*Il2*-emGFP dual reporter transgenic mice, E. Meffre (Yale University) for providing the Blimp-1 reporter mice, A. Rudensky (Memorial Sloan-Kettering Cancer Center) for providing the Foxp3–DTR–GFP mice and T.S. Simpler and U. Mudunuru for animal husbandry. This work was supported by University of Alabama at Birmingham (UAB) and National Institutes of Health grants 1R01 AI110480 to A.B.-T, R01 AI116584 to B.L, AI097357 and AI109962 to T.D.R, AIAI109962 to F.E.L and AI049360 to A.J.Z. The X-RAD 320 unit was purchased using a Research Facility Improvement Grant, 1 G20RR022807-01, from the National Center for Research Resources, National Institutes of Health. Support for the UAB flow cytometry core was provided by grants P30 AR048311 and P30 AI027767.

References

1. Yuan X, Cheng G, Malek TR. The importance of regulatory T-cell heterogeneity in maintaining self-tolerance. Immunological reviews. 2014; 259:103–114. [PubMed: 24712462]
2. Lio CW, Hsieh CS. A two-step process for thymic regulatory T cell development. Immunity. 2008; 28:100–111. [PubMed: 18199417]
3. Burchill MA, Yang J, Vogtenhuber C, Blazar BR, Farrar MA. IL-2 receptor beta-dependent STAT5 activation is required for the development of Foxp3+ regulatory T cells. J Immunol. 2007; 178:280–290. [PubMed: 17182565]

4. Yao Z, et al. Nonredundant roles for Stat5a/b in directly regulating Foxp3. Blood. 2007; 109:4368–4375. [PubMed: 17227828]
5. Fontenot JD, Rasmussen JP, Gavin MA, Rudensky AY. A function for interleukin 2 in Foxp3-expressing regulatory T cells. Nature immunology. 2005; 6:1142–1151. [PubMed: 16227984]
6. D'Cruz LM, Klein L. Development and function of agonist-induced CD25+Foxp3+ regulatory T cells in the absence of interleukin 2 signaling. Nature immunology. 2005; 6:1152–1159. [PubMed: 16227983]
7. Cheng G, Yu A, Dee MJ, Malek TR. IL-2R signaling is essential for functional maturation of regulatory T cells during thymic development. J Immunol. 2013; 190:1567–1575. [PubMed: 23315074]
8. de la Rosa M, Rutz S, Dorninger H, Scheffold A. Interleukin-2 is essential for CD4+CD25+ regulatory T cell function. European journal of immunology. 2004; 34:2480–2488. [PubMed: 15307180]
9. Sadlack B, et al. Ulcerative colitis-like disease in mice with a disrupted interleukin-2 gene. Cell. 1993; 75:253–261. [PubMed: 8402910]
10. Leon B, Bradley JE, Lund FE, Randall TD, Ballesteros-Tato A. FoxP3+ regulatory T cells promote influenza-specific Tfh responses by controlling IL-2 availability. Nature communications. 2014; 5:3495.
11. Pandiyan P, Zheng L, Ishihara S, Reed J, Lenardo MJ. CD4+CD25+Foxp3+ regulatory T cells induce cytokine deprivation-mediated apoptosis of effector CD4+ T cells. Nature immunology. 2007; 8:1353–1362. [PubMed: 17982458]
12. Chen Y, et al. Foxp3(+) regulatory T cells promote T helper 17 cell development in vivo through regulation of interleukin-2. Immunity. 2011; 34:409–421. [PubMed: 21435588]
13. Shevach EM. Mechanisms of foxp3+ T regulatory cell-mediated suppression. Immunity. 2009; 30:636–645. [PubMed: 19464986]
14. Johnston RJ, Choi YS, Diamond JA, Yang JA, Crotty S. STAT5 is a potent negative regulator of TFH cell differentiation. The Journal of experimental medicine. 2012; 209:243–250. [PubMed: 22271576]
15. Nurieva RI, et al. STAT5 protein negatively regulates T follicular helper (Tfh) cell generation and function. The Journal of biological chemistry. 2012; 287:11234–11239. [PubMed: 22318729]
16. Ballesteros-Tato A, et al. Interleukin-2 inhibits germinal center formation by limiting T follicular helper cell differentiation. Immunity. 2012; 36:847–856. [PubMed: 22464171]
17. Smigiel KS, et al. CCR7 provides localized access to IL-2 and defines homeostatically distinct regulatory T cell subsets. The Journal of experimental medicine. 2014; 211:121–136. [PubMed: 24378538]
18. Gratz IK, et al. Cutting Edge: memory regulatory t cells require IL-7 and not IL-2 for their maintenance in peripheral tissues. J Immunol. 2013; 190:4483–4487. [PubMed: 23543753]
19. Raynor J, et al. IL-15 Fosters Age-Driven Regulatory T Cell Accrual in the Face of Declining IL-2 Levels. Frontiers in immunology. 2013; 4:161. [PubMed: 23805138]
20. Chung Y, et al. Follicular regulatory T cells expressing Foxp3 and Bcl-6 suppress germinal center reactions. Nature medicine. 2011; 17:983–988.
21. Linterman MA, et al. Foxp3+ follicular regulatory T cells control the germinal center response. Nature medicine. 2011; 17:975–982.
22. Wollenberg I, et al. Regulation of the germinal center reaction by Foxp3+ follicular regulatory T cells. J Immunol. 2011; 187:4553–4560. [PubMed: 21984700]
23. Sage PT, Francisco LM, Carman CV, Sharpe AH. The receptor PD-1 controls follicular regulatory T cells in the lymph nodes and blood. Nature immunology. 2013; 14:152–161. [PubMed: 23242415]
24. Sage PT, Paterson AM, Lovitch SB, Sharpe AH. The coinhibitory receptor CTLA-4 controls B cell responses by modulating T follicular helper, T follicular regulatory, and T regulatory cells. Immunity. 2014; 41:1026–1039. [PubMed: 25526313]
25. Wing JB, Ise W, Kurosaki T, Sakaguchi S. Regulatory T cells control antigen-specific expansion of Tfh cell number and humoral immune responses via the coreceptor CTLA-4. Immunity. 2014; 41:1013–1025. [PubMed: 25526312]

26. Oestreich KJ, Mohn SE, Weinmann AS. Molecular mechanisms that control the expression and activity of Bcl-6 in TH1 cells to regulate flexibility with a TFH-like gene profile. Nature immunology. 2012; 13:405–411. [PubMed: 22406686]
27. Levin AM, et al. Exploiting a natural conformational switch to engineer an interleukin-2 'superkine'. Nature. 2012; 484:529–533. [PubMed: 22446627]
28. Aloulou M, et al. Follicular regulatory T cells can be specific for the immunizing antigen and derive from naive T cells. Nature communications. 2016; 7:10579.
29. Wang L, et al. Key role for IL-21 in experimental autoimmune uveitis. Proceedings of the National Academy of Sciences of the United States of America. 2011; 108:9542–9547. [PubMed: 21593413]
30. Malek TR, Yu A, Vincek V, Scibelli P, Kong L. CD4 regulatory T cells prevent lethal autoimmunity in IL-2Rbeta-deficient mice. Implications for the nonredundant function of IL-2. Immunity. 2002; 17:167–178. [PubMed: 12196288]
31. Zheng SG, Wang J, Wang P, Gray JD, Horwitz DA. IL-2 is essential for TGF-beta to convert naive CD4+CD25− cells to CD25+Foxp3+ regulatory T cells and for expansion of these cells. J Immunol. 2007; 178:2018–2027. [PubMed: 17277105]
32. Davidson TS, DiPaolo RJ, Andersson J, Shevach EM. Cutting Edge: IL-2 is essential for TGF-beta-mediated induction of Foxp3+ T regulatory cells. J Immunol. 2007; 178:4022–4026. [PubMed: 17371955]
33. Koch MA, et al. The transcription factor T-bet controls regulatory T cell homeostasis and function during type 1 inflammation. Nature immunology. 2009; 10:595–602. [PubMed: 19412181]
34. Bedoya F, et al. Viral antigen induces differentiation of Foxp3+ natural regulatory T cells in influenza virus-infected mice. J Immunol. 2013; 190:6115–6125. [PubMed: 23667113]
35. Cretney E, et al. The transcription factors Blimp-1 and IRF4 jointly control the differentiation and function of effector regulatory T cells. Nature immunology. 2011; 12:304–311. [PubMed: 21378976]
36. Hollister K, et al. Insights into the role of Bcl6 in follicular Th cells using a new conditional mutant mouse model. J Immunol. 2013; 191:3705–3711. [PubMed: 23980208]
37. Rubtsov YP, et al. Regulatory T cell-derived interleukin-10 limits inflammation at environmental interfaces. Immunity. 2008; 28:546–558. [PubMed: 18387831]
38. Victora GD, Nussenzweig MC. Germinal centers. Annual review of immunology. 2012; 30:429–457.
39. Maceiras AR, et al. T follicular helper and T follicular regulatory cells have different TCR specificity. Nature communications. 2017; 8:15067.
40. Hsieh CS, Lee HM, Lio CW. Selection of regulatory T cells in the thymus. Nature reviews Immunology. 2012; 12:157–167.
41. Hsieh CS, Zheng Y, Liang Y, Fontenot JD, Rudensky AY. An intersection between the self-reactive regulatory and nonregulatory T cell receptor repertoires. Nature immunology. 2006; 7:401–410. [PubMed: 16532000]
42. Wu WW, Sun YH, Pante N. Nuclear import of influenza A viral ribonucleoprotein complexes is mediated by two nuclear localization sequences on viral nucleoprotein. Virol J. 2007; 4:49. [PubMed: 17547769]
43. Avalos AM, Busconi L, Marshak-Rothstein A. Regulation of autoreactive B cell responses to endogenous TLR ligands. Autoimmunity. 2010; 43:76–83. [PubMed: 20014959]
44. Mandal M, et al. Epigenetic repression of the Igk locus by STAT5-mediated recruitment of the histone methyltransferase Ezh2. Nature immunology. 2011; 12:1212–1220. [PubMed: 22037603]
45. Walker SR, Nelson EA, Frank DA. STAT5 represses BCL6 expression by binding to a regulatory region frequently mutated in lymphomas. Oncogene. 2007; 26:224–233. [PubMed: 16819511]
46. McDonald PW, et al. IL-7 signalling represses Bcl-6 and the TFH gene program. Nature communications. 2016; 7:10285.
47. Vang KB, et al. IL-2, -7, and -15, but not thymic stromal lymphopoeitin, redundantly govern CD4+Foxp3+ regulatory T cell development. J Immunol. 2008; 181:3285–3290. [PubMed: 18714000]

48. Bayer AL, Lee JY, de la Barrera A, Surh CD, Malek TR. A function for IL-7R for CD4+CD25+Foxp3+ T regulatory cells. J Immunol. 2008; 181:225–234. [PubMed: 18566388]

49. Rangel-Moreno J, et al. The development of inducible bronchus-associated lymphoid tissue depends on IL-17. Nature immunology. 2011; 12:639–646. [PubMed: 21666689]

50. Lee BO, et al. CD4 T cell-independent antibody response promotes resolution of primary influenza infection and helps to prevent reinfection. Journal of immunology. 2005; 175:5827–5838.

51. Lim WK, Lyashenko E, Califano A. Master regulators used as breast cancer metastasis classifier. Pac Symp Biocomput. 2009:504–515. [PubMed: 19209726]

52. Carro MS, et al. The transcriptional network for mesenchymal transformation of brain tumours. Nature. 2010; 463:318–325. [PubMed: 20032975]

53. Bar-Joseph Z, Gifford DK, Jaakkola TS. Fast optimal leaf ordering for hierarchical clustering. Bioinformatics. 2001; 17(Suppl 1):S22–29. [PubMed: 11472989]

54. Eisen MB, Spellman PT, Brown PO, Botstein D. Cluster analysis and display of genome-wide expression patterns. Proceedings of the National Academy of Sciences of the United States of America. 1998; 95:14863–14868. [PubMed: 9843981]

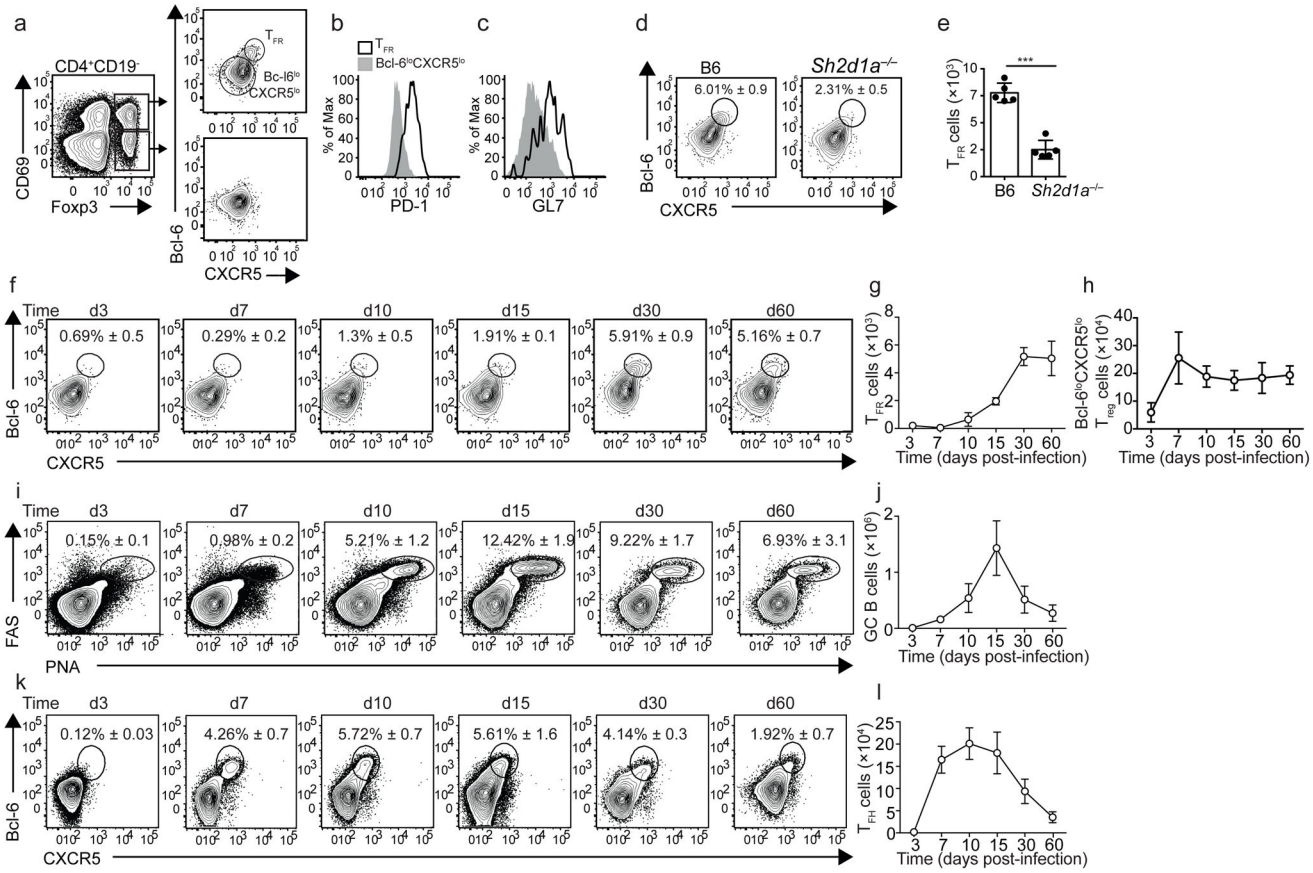

Figure 1. Kinetic of the T_{FR} cell response to influenza

(A–C) B6 mice were infected with PR8 and cells from the mLN were analyzed on day 30 after infection by flow cytometry. **(A)** Expression of Bcl-6 and CXCR5 in FoxP3^{+}CD69^{hi} and FoxP3^{+}CD69^{lo} CD4^{+} T cells. Expression of PD-1 **(B)** and GL-7 **(C)** on Bcl-6^{lo}CXCR5^{lo} and Bcl-6^{hi}CXCR5^{hi} FoxP3^{+}CD69^{hi} CD4^{+} T cells. Data are representative of five independent experiments (3–5 mice per experiment). **(D–E)** B6 and B6.*Sh2d1a*$^{-/-}$ mice were infected with PR8 and the frequency **(D)** and number **(E)** of FoxP3^{+}CD69^{hi}CD4^{+} T cells with a Bcl-6^{hi}CXCR5^{hi} T_{FR} cell phenotype were evaluated in the mLN on day 30 after infection. Data are representative of three independent experiments (mean ± SD of 3–5 mice per group). *P < 0.05, **P < 0.01, ***P < 0.001. P values were determined using a two-tailed Student's t-test. **(F–I)** B6 mice were infected with PR8 and cells from the mLN were analyzed by flow cytometry at the indicated time-points. Frequency **(F)** and number **(G)** of Bcl-6^{hi}CXCR5^{hi} T_{FR} cells. Representative plots were gated on FoxP3^{+}CD69^{hi}CD19^{-} CD4^{+} T cells. **(H)** Number of FoxP3^{+}CD69^{hi} T_{reg} cells with a Bcl-6^{lo}CXCR5^{lo} phenotype. Frequency **(I)** and number (**J**) of CD19+CD138–PNA^{hi}CD95^{hi} GC B cells. Frequency **(K)** and number (**L**) of Bcl-6hiCXCR5hi T_{FH} cells. Representative plots were gated on CD4^{+}FoxP3^{-}CD19^{-}T cells. Data are shown as the mean ± SD (n=4–5 mice/time point). Data are representative of three independent experiments. *P < 0.05, **P < 0.01, ***P < 0.001. P values were determined using a two-tailed Student's t-test.

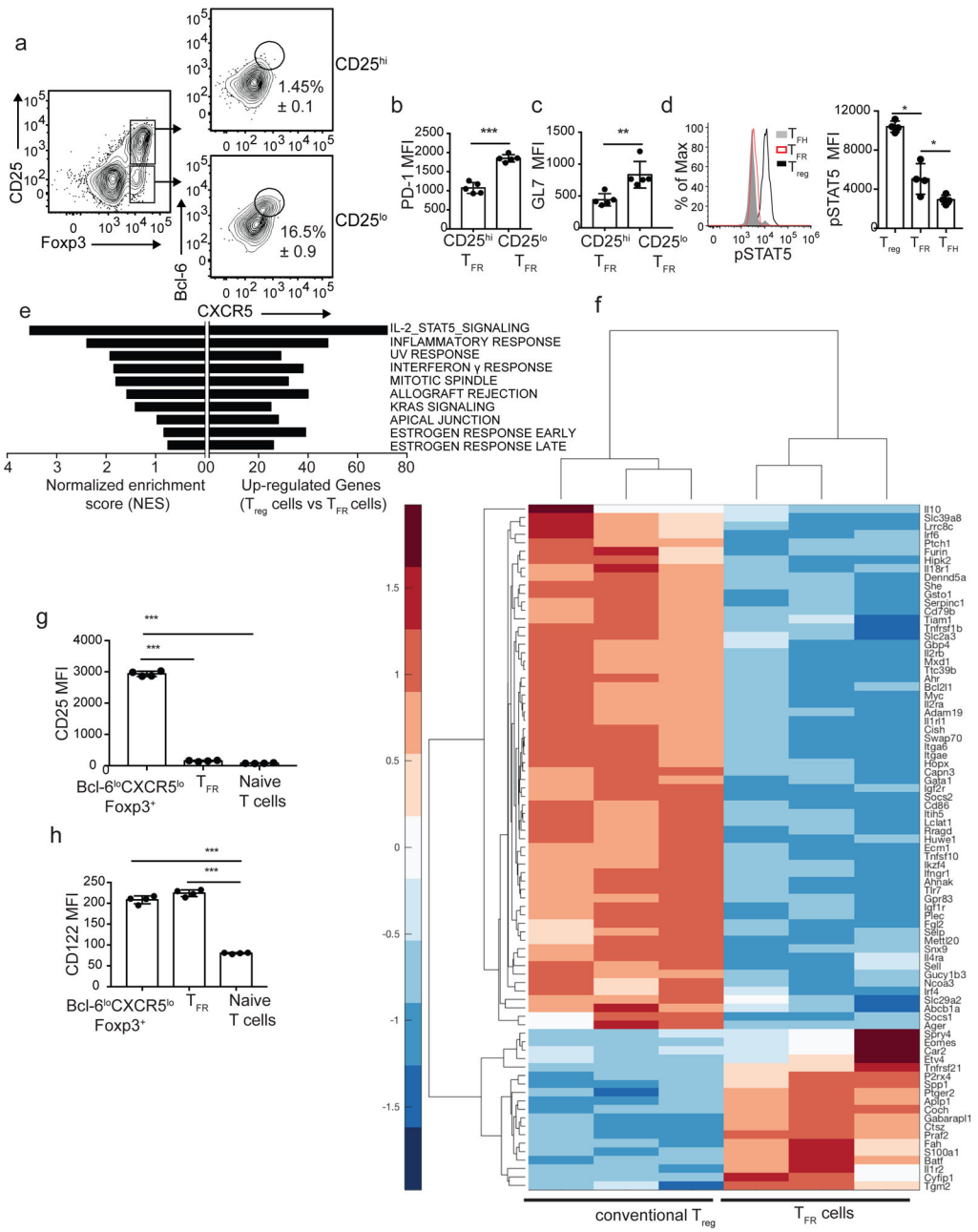

Figure 2. T_{FR} cells are $CD25^{lo}$

(A–E) B6 mice were infected with PR8 and cells from the mLN were analyzed on day 30 by flow cytometry. **(A)** Frequency of $CD25^{hi}$ and $CD25^{lo}$ $FoxP3^{+}CD69^{hi}$ $CD4^{+}$ T cells with a $Bcl\text{-}6^{hi}CXCR5^{hi}$ phenotype. Expression of PD-1 **(B)** and GL-7 **(C)** in $CD25^{hi}$ and $CD25^{lo}$ $Bcl\text{-}6^{hi}CXCR5^{hi}$ cells. Data are representative of five independent experiments. Data are shown as the mean ± SD (n=4 mice). P values were determined using a two-tailed Student's t-test. **(D)** B6 mice were infected with PR8 and STAT5 phosphorylation in $CD4^{+}B220^{-}CD25^{lo}Bcl\text{-}6^{hi}CXCR5^{hi}$ $Foxp3^{+}$ T_{FR} cells, $CD4^{+}B220^{-}CD25^{hi}Bcl\text{-}6^{lo}CXCR5^{lo}Foxp3^{+}$ conventional T_{reg} cells and

$CD4^+B220^-Bcl\text{-}6^{hi}CXCR5^{hi}$ $Foxp3^-$ T_{FH} cells was determined by flow cytometry on day 15. Cells were stimulated with 100ng/ml of rIL-2 for 15 minutes before analyzing staining. Data are representative of two independent experiments. Data are shown as the mean ± SD (n=4 mice). *P < 0.05, **P < 0.01, ***P < 0.001. P values were determined using a two-tailed Student's t-test. **(E–F)** Conventional T_{reg} cells ($CD19^-CD4^+FoxP3^+CD69^{hi}PD\text{-}1^{lo}CXCR5^{lo}CD25^{hi}$) and T_{FR} cells ($CD19^-CD4^+FoxP3^+CD69^{hi}PD\text{-}1^{hi}CXCR5^{hi}CD25^{lo}$) were sorted from the mLN of FoxP3–DTR–GFP at day 30 after infection and RNA-seq was performed. **(E)** Gene set enrichment analysis (GSEA, Broad Institute) examining differentially expressed genes between T_{reg} cells and T_{FR} cells (adjusted p-value <0.05, Log2fold change greater than or equal to 1. The Normalized Enriched Score (NES) and the number of up-regulated genes for each of the top 10 Hallmark -signaling Pathways resulting from the GSEA analysis are shown. **(F)** Heatmap displaying the expression of the IL-2–STAT5 Hallmark-signaling pathway genes that are differentially expressed in conventional T_{reg} cells relative to T_{FR} cells. Three replicates for each cell type were obtained from three independent experiments. **(G and H)** Expression of CD25 **(G)** and CD122 **(H)** in $Bcl\text{-}6^{lo}CXCR5^{lo}$ $FoxP3^+CD69^{hi}$ $CD4^+$ T cells, $Bcl\text{-}6^{hi}CXCR5^{hi}$ T_{FR} cells and $CD44^{lo}CD69^{lo}FoxP3^-$ $CD4^+$ T cells (naïve). Data are representative of two independent experiments. Data are shown as the mean ± SD (n=5 mice). *P < 0.05, **P < 0.01, ***P < 0.001. P values were determined using a two-tailed Student's t-test.

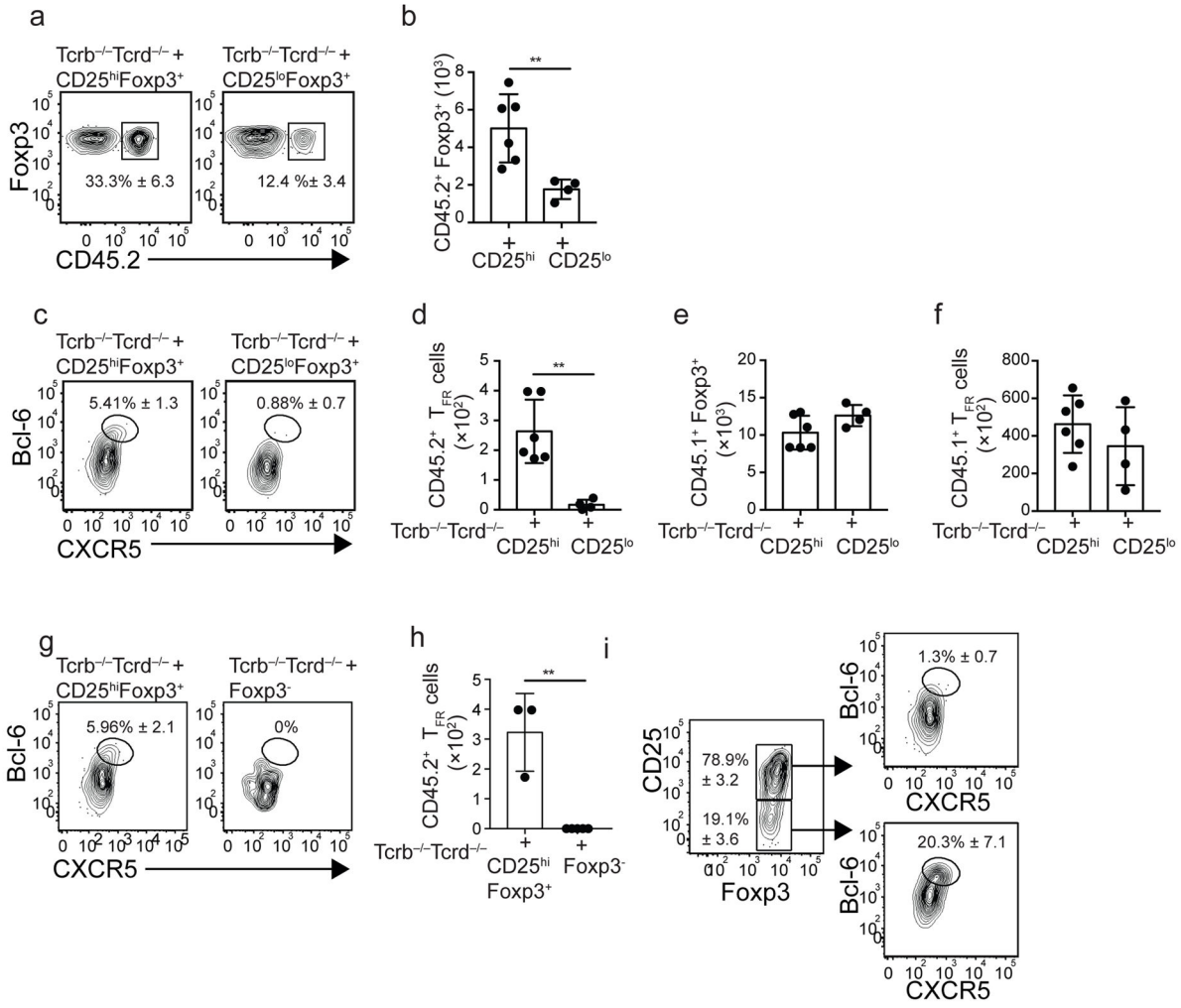

Figure 3. CD25$^+$FoxP3$^+$ T$_{reg}$ cells down-regulate CD25 and differentiate into T$_{FR}$ cells

(A–F) Equivalent numbers of sorted CD25^{hi}FoxP3$^+$ and CD25^{lo}FoxP3$^+$ CD4$^+$ T cells obtained from the spleens of naïve CD45.2$^+$ B6-Foxp3-DTR–GFP mice were adoptively transferred into *Tcrb*$^{-/-}$ *Tcrd*$^{-/-}$ recipient mice. Recipient mice also received purified CD4$^+$ and CD8$^+$ T cells from the spleen of naïve CD45.1$^+$ B6 mice. One day later, recipient mice were infected with influenza and donor-derived CD45.2$^+$ (**A–D**) and donor-derived CD45.1$^+$ **(E–F)** CD69$^+$FoxP3$^+$CD4$^+$ T cells were assessed in the mLN on day 30 by flow cytometry. The frequency **(A)** and number **(B)** of CD45.2$^+$FoxP3$^+$ cells in recipients receiving CD25^{hi}FoxP3$^+$ and CD25^{lo}FoxP3$^+$ cells are shown. Plots were gated on FoxP3$^+$CD69^{hi}CD4$^+$ T cells. The frequency **(C)** and number **(D)** of CD45.2$^+$CD69$^+$FoxP3$^+$ CD4$^+$ T cells with a Bcl-6^{hi}CXCR5^{hi} phenotype in recipients receiving CD25^{hi}FoxP3$^+$ and CD25^{lo}FoxP3$^+$ cells are shown. **(E)** The number of donor-derived CD45.1$^+$CD69$^+$FoxP3$^+$CD4$^+$ T cells in recipients receiving CD25^{hi}FoxP3$^+$ and CD25^{lo}FoxP3$^+$ cells are shown. **(F)** The number of donor-derived CD45.1$^+$CD69$^+$FoxP3$^+$ T cells with a Bcl-6^{hi}CXCR5^{hi} phenotype in recipients receiving CD25^{hi}FoxP3$^+$ and CD25^{lo}FoxP3$^+$ cells are shown. Data were pooled from two independent experiments (mean ± SD). *P < 0.05, **P < 0.01, ***P < 0.001. P values were determined using a two-tailed

Student's t-test. **(G–H)** Equivalent numbers of sorted $CD25^{hi}FoxP3^{+}$ and $FoxP3^{-}$ $CD4^{+}$ T cells obtained from the spleen of naïve $CD45.2^{+}$ B6-Foxp3-DTR–GFP mice were adoptively transferred into *Tcrb*$^{-/-}$ *Tcrd*$^{-/-}$ recipient mice. The recipient mice also received purified $CD4^{+}$ and $CD8^{+}$ T cells from the spleen of naïve $CD45.1^{+}$ B6 mice. One day later, the mice were infected with influenza and the donor-derived $CD45.2^{+}$ $CD69^{+}FoxP3^{+}CD4^{+}$ T cells were assessed in the mLN on day 30 by flow cytometry. Frequency **(G)** and number **(H)** of $CD45.2^{+}CD69^{+}FoxP3^{+}$ T cells with a $Bcl\text{-}6^{hi}CXCR5^{hi}$ phenotype in recipients of $CD25^{hi}FoxP3^{+}$ and $FoxP3^{-}CD4^{+}$ T cells. **(I)** Frequencies of $Bcl\text{-}6^{hi}CXCR5^{hi}$ in $CD25^{hi}$ and $CD25^{lo}$ $FoxP3^{+}$ cells derived from the $CD45.2^{+}CD25^{hi}Foxp3^{+}$ donors. Data are representative of two independent experiments. Data are shown as the mean ± SD (n=3–5 mice). *P < 0.05, **P < 0.01, ***P < 0.001. P values were determined using a two-tailed Student's t-test.

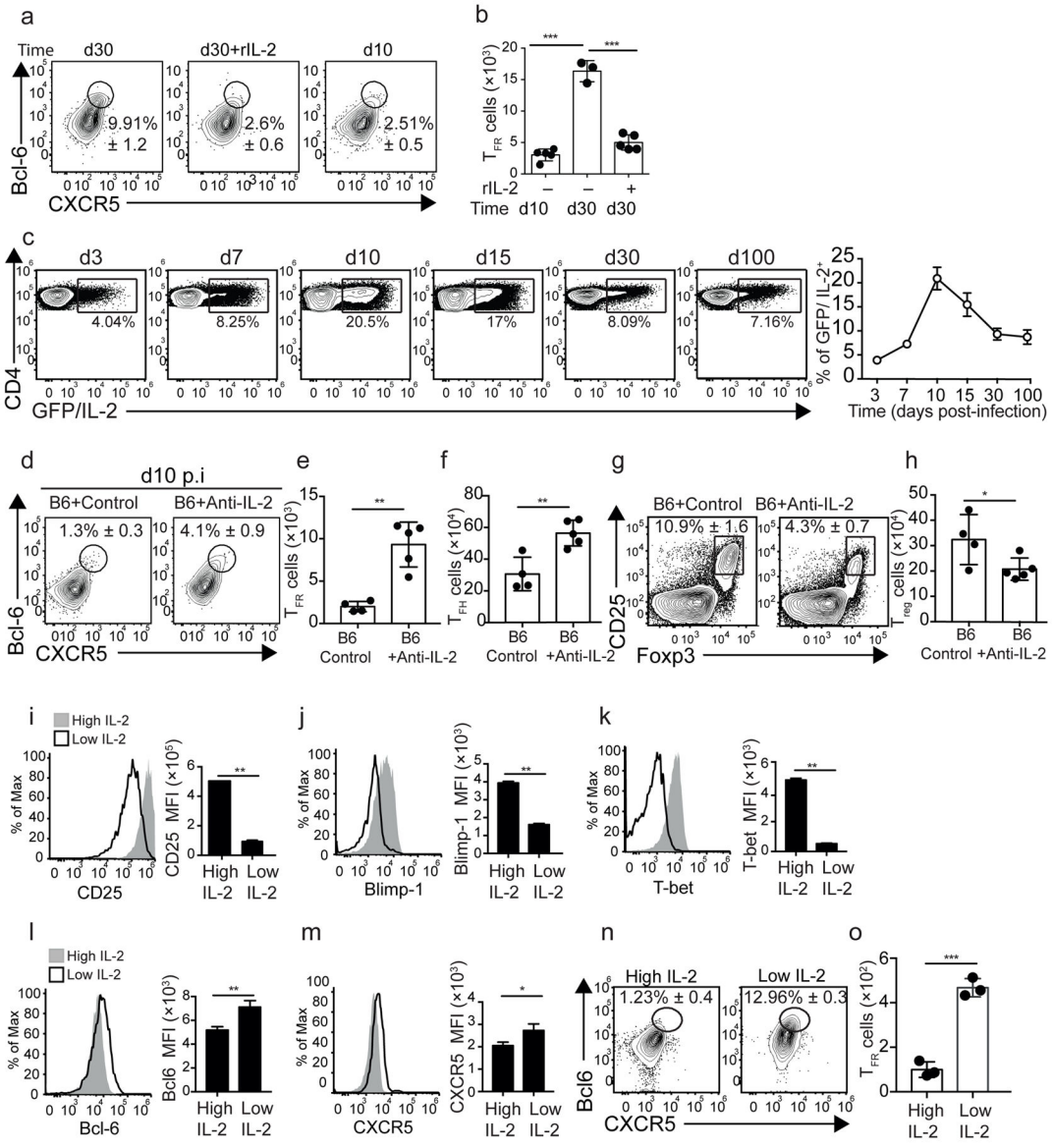

Figure 4. IL-2 inhibits T_{FR} cell differentiation

(A–B) B6 mice were infected with PR8 and treated daily with 30,000 U of rIL-2 or PBS starting on day 20. Cells from the mLNs were analyzed by flow cytometry on day 30. As a control, cells from the mLNs of day 10 infected mice are also shown. The frequency (**A)** and number **(B)** of $CD25^{lo}FoxP3^{+}$ $CD4^{+}$ T cells with a $Bcl\text{-}6^{hi}CXCR5^{hi}$ phenotype. Data are representative of three independent experiments. Data are shown as the mean ± SD (n=3–5 mice per group). *P < 0.05, **P < 0.01, ***P < 0.001. P values were determined using a two-tailed Student's t-test. **(C)** *Il21*-mCherry-*Il2*-emGFP mice were infected with PR8 and cells from the mLN were analyzed at the indicated time-points. Representative plots were gated on $CD4^{+}$ T cells. Data are shown as the mean ± SD (n=3–5 mice per group). Data are representative of three independent experiments. **(D–H)** B6 mice were infected with PR8 and treated daily with 500 μg of a mix of anti IL-2 neutralizing Abs (JES6-1A12 + S4B6-1) or control Ab (2A3) starting on day 3 after infection. The frequency **(D)** and number **(E)** of

Bcl-6^{hi}CXCR5^{hi} T_{FR} cells were calculated on day 10 after infection. Plots were gated on FoxP3^{+}CD69^{hi}CD4^{+} T cells. **(F)** Number of Bcl-6^{hi}CXCR5^{hi} T_{FH} cells. Frequency (**G)** and number (**H**) of CD25^{hi}FoxP3^{+} cells. Plots were gated on CD4^{+} T cells. Data are representative of three independent experiments. Data are shown as the mean ± SD (n=4–5 mice per group). *P < 0.05, **P < 0.01, ***P < 0.001. P values were determined using a two-tailed Student's t-test. **(I–O)** B6.FoxP3-DTR–GFP mice were infected with PR8 and CD25^{hi}FoxP3^{+} CD4^{+} T cells were sorted from the mLN and spleens at day 7 after infection. Sorted cells were then activated with anti-CD3–CD28 beads in the presence of high (200U/ml) or low (5U/ml) IL-2 concentrations. The expression of CD25 **(I)**, Blimp-1 **(J)**, T-bet **(K)**, Bcl-6 **(L)** and CXCR5 **(M)** were assessed 72h later by flow cytometry. The frequency (**N)** and number **(O)** of FoxP3^{+} CD4^{+} T cells with a Bcl-6^{hi}CXCR5^{hi} phenotype are shown. Data are representative of three independent experiments. All values were obtained in triplicate and the data are shown as the mean ± SD. *P < 0.05, **P < 0.01, ***P < 0.001P. values were determined using a two-tailed Student's t-test.

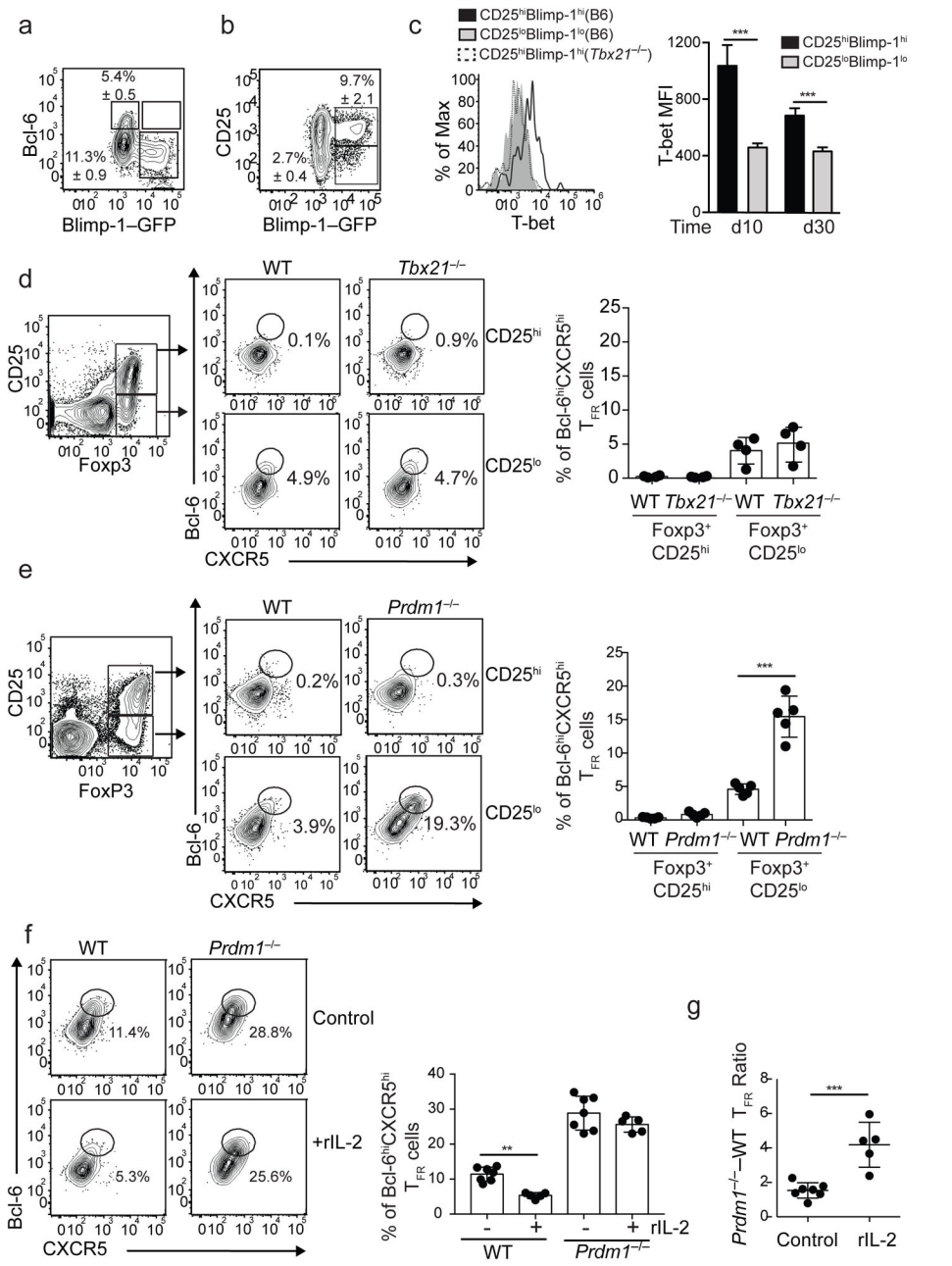

Figure 5. IL-2 inhibits T_{FR} cell differentiation by a Blimp-1 mechanism

(A–B) B6.Blimp-1/YFP reporter mice were infected with PR8 and cells from the mLN were analyzed on day 30 by flow cytometry. **(A)** Expression of Bcl-6 and Blimp-1/YFP in FoxP3^{+}CD69^{hi}CD4^{+} T cells. **(B)** Expression of CD25 and Blimp-1/YFP in FoxP3^{+}CD69^{hi}CD4^{+} T cells. Data are representative of three independent experiments (mean ± S.D of 3–5 mice per group). **(C)** B6 and *Tbx21*$^{-/-}$mice were infected with PR8 and the expression of T-bet in CD25^{hi}Blimp^{hi} and CD25^{lo}Blimp^{lo} FoxP3^{+}CD69^{hi}CD4^{+} T cells was analyzed at days 10 and 30 by intracellular staining. Data are representative of two independent experiments (mean ± S.D of 3–5 mice per group). *P < 0.05, **P < 0.01, ***P

< 0.001. P values were determined using a two-tailed Student's t-test. **(D)** *Tcrb*$^{-/-}$ *Tcrd*$^{-/-}$ mice were irradiated and reconstituted with a 50:50 mix of BM from CD45.1^{+} WT and CD45.2^{+} *Tbx21*$^{-/-}$ donors. Eight weeks later, reconstituted mice were infected with PR8 and cells from the mLN were analyzed on day 10. The frequency of CD25^{lo}FoxP3^{+} and CD25^{hi}FoxP3^{+} cells with a Bcl-6^{hi}CXCR5^{hi} phenotype was determined in the CD45.1^{+} and CD45.2^{+} compartments. Representative plots are shown. Data in the graph are shown as the mean ± SD (n=4 mice). Data are representative of two independent experiments. **(E)** *Tcrb*$^{-/-}$ *Tcrd*$^{-/-}$ mice were irradiated and reconstituted with a 50:50 mix of BM from CD45.1^{+} WT and CD45.2^{+} *Prdm1*$^{fl/fx}$-*Lck*$^{cre/+}$ donors. Eight weeks later, reconstituted mice were infected with PR8 and cells from the mLN were analyzed on day 10. The frequency of CD25^{lo}FoxP3^{+} and CD25^{hi}FoxP3^{+} cells with a Bcl-6^{hi}CXCR5^{hi} phenotype were calculated in the CD45.1^{+} and CD45.2^{+} compartments. Representative plots are shown. Data in the graph are shown as the mean ± SD (n=5 mice). Data are representative of three independent experiments. *P < 0.05, **P < 0.01, ***P < 0.001. P values were determined using a two-tailed Student's t-test. **(F–G)** WT-*Prdm1*$^{fl/fl}$-*Lck*$^{cre/+}$ chimeric mice were infected with PR8 and treated daily with 30,000 U of rIL-2 or PBS (control) starting 20 days after infection. Cells from the mLNs were analyzed by flow cytometry on day 30. **(F)** Frequency of CD45.1^{+} and CD45.2^{+} CD25^{lo}FoxP3^{+} CD4^{+} T cells with a Bcl-6^{hi}CXCR5^{hi} T_{FR}-cell phenotype. Data in the graph are shown as the mean ± SD (n=5–7 mice/group). Representative plots are shown. **(G)** Ratio of *Prdm1*$^{-/-}$ to WT T_{FR} cell was calculated in control and rIL-2-treated mice. Data are shown as the mean ± SD (n=5–7 mice/group). Data are representative of two independent experiments. *P < 0.05, **P < 0.01, ***P < 0.001. P values were determined using a two-tailed Student's t-test.

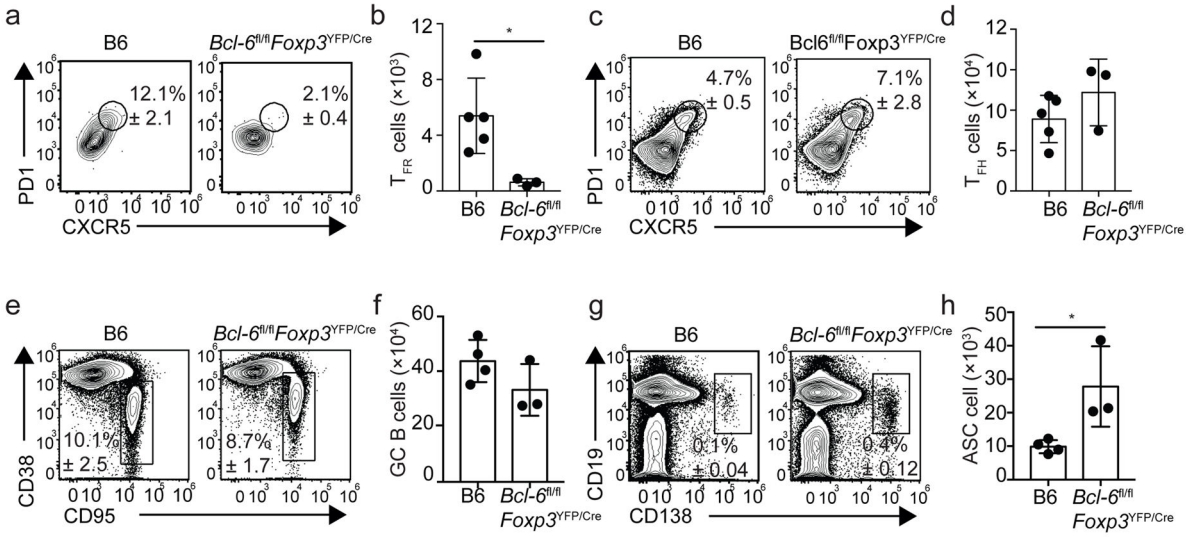

Figure 6. Abnormal expansion of CD138^{+} ASCs in the absence of T_{FR} cells

(A–H) B6 and Bcl-6$^{fl/fl}$Foxp3$^{YFP/Cre}$ mice were infected with PR8 and cells from the mLN were analyzed by flow cytometry at day 30. Frequency **(A)** and number **(B)** of PD-1^{hi}CXCR5^{hi} T_{FR} cells. Representative plots were gated on FoxP3^{+}CD69^{hi}CD25^{lo}CD19^{-} CD4^{+} T cells. Frequency **(C)** and number **(D)** of PD-1^{hi}CXCR5^{hi} T_{FH} cells. Representative plots were gated on FoxP3^{-}CD19^{-} CD4^{+} T cells. Frequency **(E)** and number **(F)** of CD19+CD138–GL-7^{+}CD38^{lo}CD95^{hi} GC B cells. Frequency **(G)** and number **(H)** of CD138^{+} ASCs. Data are shown as the mean ± SD (n=3–5 mice/group). Data are representative of three independent experiments. *P < 0.05, **P < 0.01, ***P < 0.001. P values were determined using a two-tailed Student's t-test.

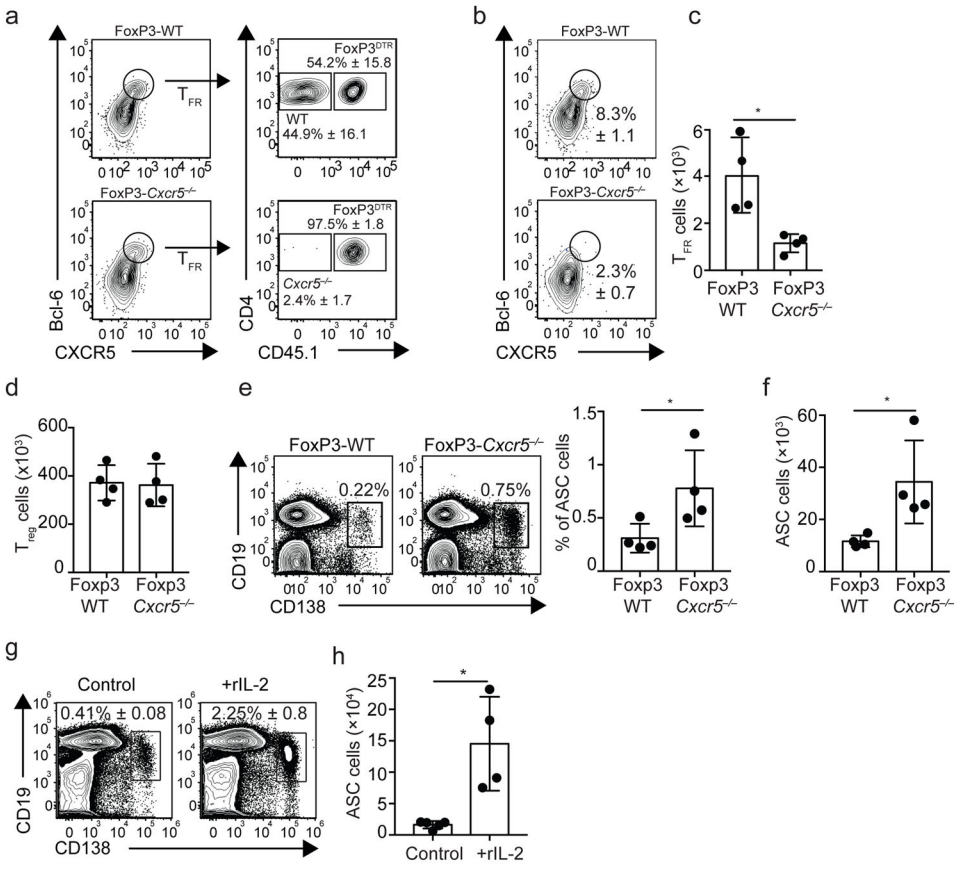

Figure 7. CD138$^+$ ASCs accumulate in T_{FR} cell depleted mice

(A–F) *Tcrb*$^{-/-}$ *Tcrd*$^{-/-}$ mice were irradiated and reconstituted with a 50:50 mix of BM from CD45.1$^+$ FoxP3-DTR and CD45.2$^+$ B6 donors (FoxP3-WT) or from CD45.1$^+$ FoxP3-DTR and CD45.2$^+$ *Cxcr5*$^{-/-}$donors (FoxP3-*Cxcr5*$^{-/-}$). **(A)** Reconstituted FoxP3-WT and FoxP3-*Cxcr5*$^{-/-}$chimeras were infected with PR8 and the frequency of CD45.1$^+$ and CD45.2$^+$ cells within the FoxP3$^+$CD69^{hi}CD25^{lo} T_{FR} cell population was calculated on day 50. **(B–F)** Reconstituted FoxP3-WT and FoxP3- *Cxcr5*$^{-/-}$ chimeras were infected with PR8, treated with DT every four days starting 20 days after infection, and cells from the mLN were analyzed on day 50. Frequency **(B)** and number **(C)** of Bcl-6^{hi}CXCR5^{hi} T_{FR} cells. Representative plots were gated on FoxP3$^+$CD25^{lo}CD19$^-$ CD4$^+$ T cells. **(D)** Number of conventional CD25$^+$ FoxP3$^+$ T_{reg} cells. Frequency **(E)** and number **(F)** of CD138$^+$ ASCs. Data are shown as the mean ± SD (n=4–5 mice/group). Data are representative of three independent experiments. *P < 0.05, **P < 0.01, ***P < 0.001. P values were determined using a two-tailed Student's t-test. **(G–H)** B6 mice were infected with PR8 and treated daily with 15,000 U of rIL-2 or PBS starting on day 20. Cells from the mLNs were analyzed by flow cytometry on day 30. Frequency **(G)** and number **(H)** of CD138$^+$ ASCs. Data are shown as the mean ± SD (n=4–5 mice/group). Data are representative of four independent experiments. *P < 0.05, **P < 0.01, ***P < 0.001. P values were determined using a two-tailed Student's t-test.

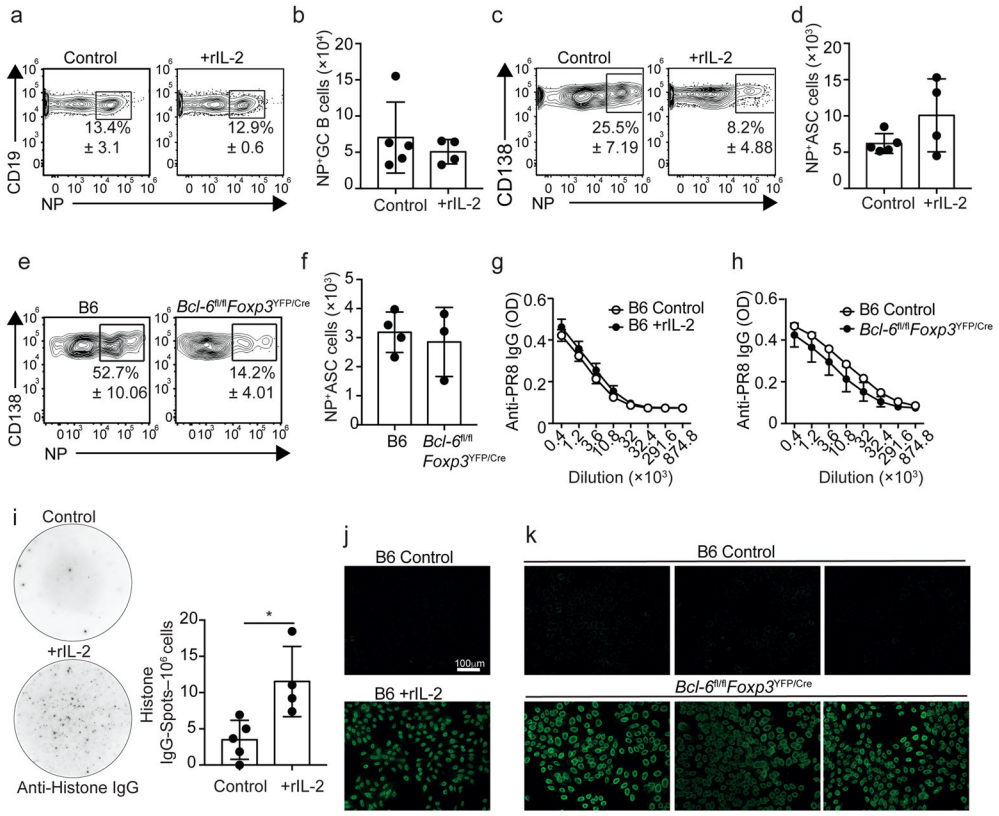

Figure 8. T_{FR} cells prevent the development of self-reactive ASC responses after infection

(A–D) B6 mice were infected with PR8 and treated daily with 15,000 U of rIL-2 or PBS starting on day 20. Cells from the mLN were analyzed by flow cytometry on day 30. Frequency **(A)** and number **(B)** of CD19+CD138–GL-7^{+}CD38^{lo}CD95^{hi} GC B cells that were NP-specific. Frequency **(C)** and number **(D)** of CD138^{+} ASCs that were influenza-NP specific. Data are shown as the mean ± SD (n=4–5 mice/group). Data are representative of four independent experiments. **(E–F)** B6 and Bcl-6$^{fl/fl}$Foxp3$^{YFP/Cre}$ mice were infected with PR8 and CD138^{+} ASCs from the mLN were analyzed by flow cytometry on day 30. Frequency **(E)** and number **(F)** of CD138^{+} ASCs that were NP-specific. Data are shown as the mean ± SD (n=3–4 mice/group). Data are representative of three independent experiments. **(G)** B6 mice were infected with PR8 and treated daily with 15,000 U of rIL-2 or PBS starting on day 20. Serum was obtained on day 30 and PR8-specific IgG Abs were measured by ELISA. Data are representative of three independent experiments (mean ± SD of 5 mice per group)**. (H)** B6 and Bcl-6$^{fl/fl}$Foxp3$^{YFP/Cre}$ mice were infected with PR8. Serum from was obtained on day 30 and PR8-specific IgG Abs were measured by ELISA. **(I)** B6 mice were infected with PR8 and treated daily with 15,000 U of rIL-2 or PBS starting 20 days after infection. Histone-specific IgG-secreting cells in the mLN were enumerated by ELISPOT on day 30. Data are representative of two independent experiments (mean ± SD of 4–5 mice per group). *P < 0.05, **P < 0.01, ***P < 0.001. All P values were determined using a two-tailed Student's t-test. **(J)** The presence of ANAs in the serum from day 30 influenza-infected control and IL-2-treated mice was determined by fluorescence microscopy using HEp-2 slides. Images are representative of two independent experiments

(n=4–5 mice/group). **(K)** ANAs in the serum from day 30 influenza-infected B6 and Bcl-6$^{fl/fl}$Foxp3$^{YFP/Cre}$ mice. Images are representative of three independent experiments (n=4–5 mice/group).